Sedimentary Geology 333 (2016) 50–69

Contents lists available at ScienceDirect

Sedimentary Geology

journal homepage: www.elsevier.com/locate/sedgeo

Proliferation of MISS-related microbial mats following the end-Permian mass extinction in terrestrial ecosystems: Evidence from the Lower Triassic of the Yiyang area, Henan Province, North China

Chenyi Tu [a], Zhong-Qiang Chen [a,*], Gregory J. Retallack [b], Yuangeng Huang [a], Yuheng Fang [a]

[a] State Key Laboratory of Biogeology and Environmental Geology, China University of Geosciences (Wuhan), Wuhan 430074, China
[b] Department of Geological Sciences, University of Oregon, Eugene, OR 97403, USA

ARTICLE INFO

Article history:
Received 30 October 2015
Received in revised form 11 December 2015
Accepted 11 December 2015
Available online 18 December 2015

Editor: Dr. B. Jones

Keywords:
MISS
Microbe
Terrestrial ecosystem
Early Triassic
Yiyang area
North China

ABSTRACT

Microbially induced sedimentary structures (MISSs) are commonly present in siliciclastic shallow marine settings following the end-Permian mass extinction, but have been rarely reported in the post-extinction terrestrial ecosystems. Here, we present six types of well-preserved MISSs from the upper Sunjiagou Formation and lower Liujiagou Formation of Induan (Early Triassic) age in the Yiyang area, Henan Province, North China. These MISSs include: polygonal sand cracks, worm-like structures, wrinkle structures, sponge pore fabrics, gas domes, and leveled ripple marks. Microanalysis shows that these MISSs are characterized by thin clayey laminae and filamentous mica grains arranged parallel to bedding plane as well as oriented matrix supported quartz grains, which are indicative of biogenic origin. Facies analysis suggests that the MISS-hosting sediments were deposited in a fluvial sedimentary system during the Early Triassic, including lake delta, riverbeds/point bars, and flood plain paleoenvironments. Abundant MISSs from Yiyang indicate that microbes also proliferated in terrestrial ecosystems in the aftermath of the Permian–Triassic (P–Tr) biocrisis, like they behaved in marine ecosystems. Microbial blooms, together with dramatic loss of metazoans, may reflect environmental stress and degradation of terrestrial ecosystems or arid climate immediately after the severe Permian–Triassic ecologic crisis.

1. Introduction

As a consequence of the end-Permian mass extinction, microbial proliferation characterizes the much degraded marine ecosystems (Chen and Benton, 2012). Microbial communities bloomed in shallow marine settings, in which they grew as microbialites (i.e., stromatolites, thrombolites, dendrites, and so on) in carbonate habitats (i.e., Kershaw et al., 2012; Chen et al., 2014) and various microbially induced sedimentary structures (MISS sensu Noffke et al., 2001) in siliciclastic shallow sea (Pruss et al., 2004; Mata and Bottjer, 2009a,2009b). These unusual biosedimentary structures, together with dramatic loss of metazoans, have been considered as markers of environmental stresses that may have been responsible for the biotic recovery (Chen and Benton, 2012). Both microbialites and MISS not only were widespread through the entire Early Triassic (Pruss et al., 2004, 2005, 2006; Baud et al., 2007; Ezaki et al., 2012; Kershaw et al., 2012; Chen et al., 2014), but also occurred occasionally in earliest Middle Triassic just prior to final recovery of marine ecosystems in middle-late Anisian (Luo et al., 2013, 2014). MISS therefore is a useful sedimentary indication of ecosystem devastation in siliciclastic substrate following major mass extinctions (Mata and Bottjer, 2009a,2009b).

Most of these unusual biosedimentary structures have been reported from shallow marine settings following major biotic extinctions (Calner, 2005; Mata and Bottjer, 2009a), but some examples of MISS (Chu et al., 2015) and stromatolites (Kalkowsky, 1908; Riding, 1999) have been reported from shallow lacustrine ecosystems. Although life on land suffered at least a loss of 70% species (Erwin, 2006) and terrestrial ecosystems were severely devastated (Benton et al., 2004) in the end-Permian mass extinction, few Early Triassic non-marine stromatolites are known (Kalkowsky, 1908; Riding, 1999) and calcareous paleosol sequences through Permian and Triassic extinctions so not show unusual forms of caliche (Retallack, 2013). Siliciclastic MISSs therefore are one of most important proxies for environmental stresses in terrestrial ecosystems following major biocrises.

Given that MISSs are commonly present in the Early Triassic marine siliciclastic successions, they should also occur in post-extinction terrestrial siliciclastic strata since terrestrial ecosystems have also collapsed in the end-Permian crisis. This expectation was recently proved by Chu et al. (2015) who reported for the first time wrinkle structures, one of the commonest MISSs from the Lower Triassic terrestrial strata of the Yiyang area, Henan Province, North China. Chu et al.'s (2015) study

* Corresponding author.
E-mail address: zhong.qiang.chen@cug.edu.cn (Z.-Q. Chen).

http://dx.doi.org/10.1016/j.sedgeo.2015.12.006
0037-0738/

provides the clue that the finding of more diverse MISSs in the Early Triassic terrestrial successions is possible. More recently, we also found several other kinds of MISSs in association with the reported wrinkle structures in the post-extinction succession in the same section. These MISSs still remain undescribed. Besides, additional petrographic study and micro-analysis of the Yiyang wrinkle structures (Chu et al., 2015) are needed to test their biogenicity.

Accordingly, this study aims to document various MISSs newly observed in the Lower Triassic terrestrial successions of the Yiyang area, North China by a means of conventional petrographic study and micro-analysis using Field Emission Scanning Electron Microscope (FESEM) equipped with Energy Dispersive Spectrometer (EDS), and attempts to assess their biogenicity and to probe into links between microbial proliferation and environmental stresses following the end-Permian great dying in terrestrial ecosystems.

2. Geological and stratigraphic settings

The MISSs documented below were collected from the Lower Triassic rocks of the Yiyang area, Henan Province, North China, which was an independent block located in the northern part of the Paleo-Tethys Ocean. The North China block uplifted and became terrestrial due to the amalgamation among the Qaidam, Tarim and Siberia–Mongolia paleoplates during the Middle–Late Permian (Wang, 1985). As consequence, fluvial and lacustrine facies deposits characterize the Upper Permian and Lower Triassic successions in the North China Block. In addition, terrestrial sedimentation has been strongly influenced by pronounced climatic changes over the P–Tr transition. The mixed yellow, greenish and black siliciclastics with coal measures of the Upper Permian formations are overlain by reddish sandstone and mudstone with paleosol beds of the Lower Triassic. The former may indicate mixture of humid waterlogged conditions, while the red paleosols represent well-drained floodplains of dry, transiently humid, then dry paleoclimate (Xu et al., 2004; Yu et al., 2005; Peng and Wu, 2006).

The continuous terrestrial P–Tr succession is well exposed at the Dayulin section, ~4 km south of Yiyang county town, Henan Province, North China (Fig. 1A–B). Therein, the uppermost Permian comprises the lower and middle Sunjiagou Formation, while the Lower Triassic consists of the upper Sunjiagou, Liujiagou and Heshanggou Formations (Figs. 1B, 2A, 3A).

The Sunjiagou Formation, ~75 m thick, crops out along the riverside towards the Dayulin village. Its lower part is composed of gray-greenish thick sandstone interbedded with greenish, black mudstones and coal measures, followed by reddish mudstone interbedded with thick coarse sandstone at its middle part. The upper Sunjiagou Formation is dominated by red mudstone with numerous calcareous-nodular paleosols and yellow thin- to medium-bedded fresh-water limestones. The lower and middle Sunjiagou Formation is interpreted as a deposit of lake shores and freshwater deltas, while its upper portion represents a distal fluvial setting (Zhu et al., 2007). This succession is also representative of climatic regime shift from waterlogged to well-drained (Wang, 1988; Zhu et al., 2007; Zhang et al., 2014; Xu et al., 2015).

The overlying Liujiagou Formation, 130 m thick, is dominated by massive purple and reddish quartz sandstone, with minor amounts of conglomerates, feldspar sandstone and calcareous siltstone. Well-preserved ripples and cross-bedding are common through the entire formation. This stratigraphic unit has been interpreted as the sedimentation of a fluvial system with a semi-arid climatic regime (Zhang et al., 2014; Xu et al., 2015).

The Heshanggou Formation, overlying the Liujiagou Formation, is marked by reddish mudstone and siltstone with thick paleosol layers at its lower part, massive purple quartz sandstone with minor constituents of conglomerates in the middle part, and highly bioturbated fine sandstone and siltstone in the upper part. Hu et al. (2009) interpreted this unit as the result of deposition in nearshore to shallow lacustrine to lake delta settings.

The age assignment of the Sunjiagou Formation has long been disputed. Previously, this formation was assigned to either the Late Permian (Cheng et al., 1983; Wang, 1986, 1997; Zhang, 1991; Lin and Fu, 1992; Yuan et al., 2003) or Early Triassic (Yang et al., 1979; Yin and Lin, 1979; Zhao et al., 1980; Ouyang and Zhang, 1982; Liu and Liu, 1984; Zhang et al., 1994; Liu and He, 2000; Li et al., 2003; Liu et al., 2014) in age based on faunal and floral correlations. It should be noted that Ouyang and Zhang (1982) established the *Lundbladispora–Aratrisporites–Taeniaesporites* microfloral assemblage from the upper Sunjiagou Formation. More recently, this spore assemblage has been widely treated as the first microfloral zone of the Triassic worldwide (Tewari et al., 2015; Yu et al., 2015). Accordingly, the P–Tr boundary can be placed at the upper Sunjiaogou Formation, ~20 m below the top of the formation in many sections in North China (Ouyang and Zhang, 1982), which is calibrated to the base of Bed 6 of the Sunjiagou Formation in Dayulin (Fig. 2). The Sunjiagou Formation therefore ranges from the latest Permian to earliest Triassic in age (Fig. 2).

All of the plant, microfloral, concostracan, and bivalve assemblages obtained from North China suggest a late Induan and Olenekian age for the

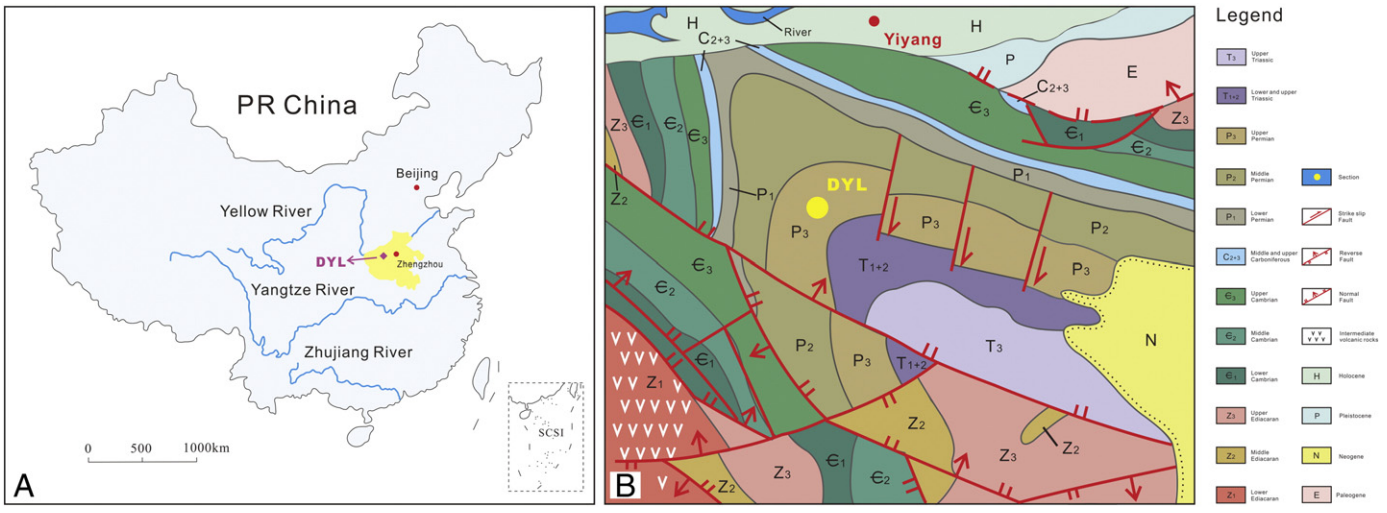

Fig. 1. (A) Index map showing the location of Henan Province (yellow area). (B) Geological map showing the regional settings of the Dayulin (DYL) section of Yiyang county, Henan Province, North China (modified from the Geological Team of the Henan Geological Bureau, 1965).

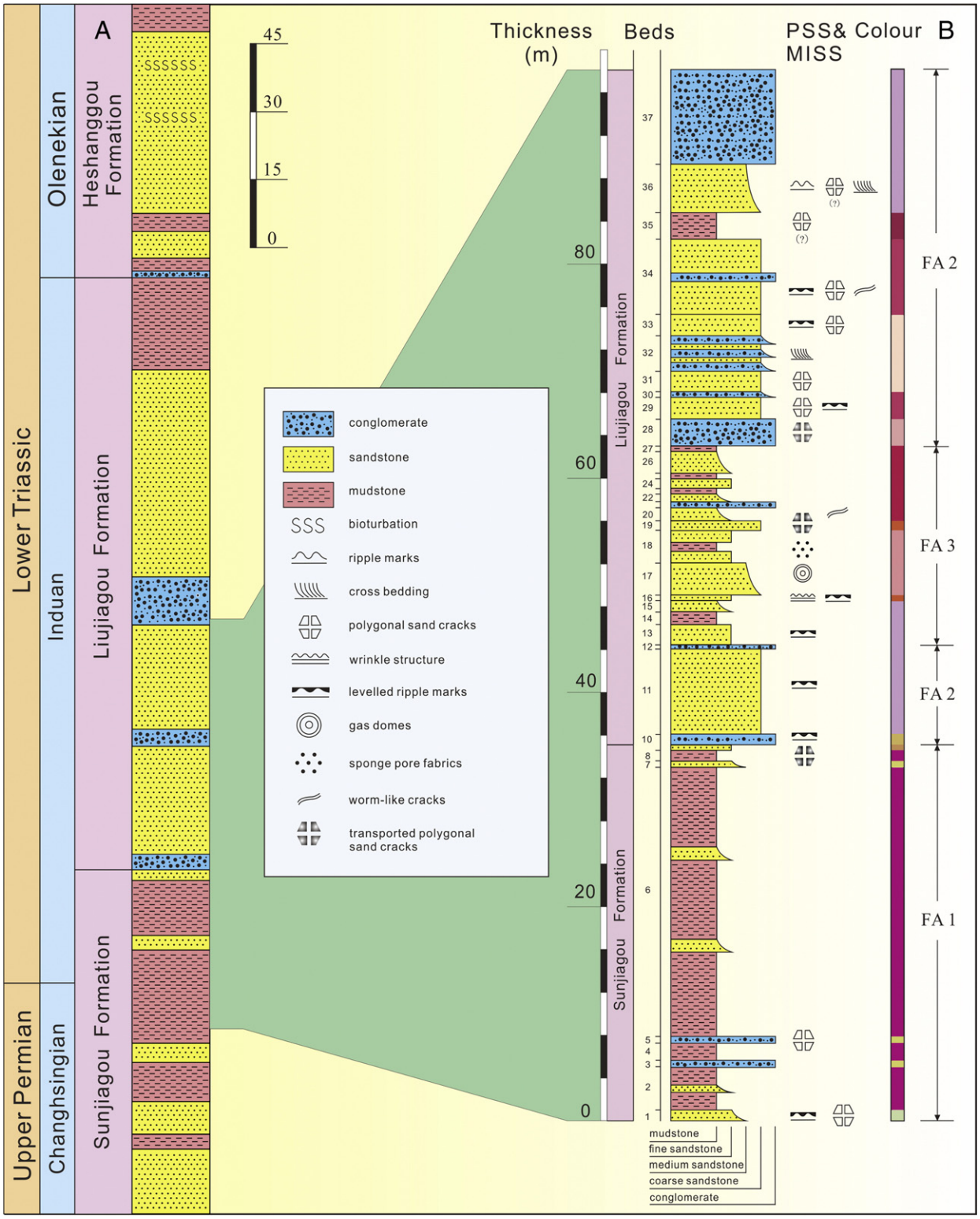

Fig. 2. (A) Composite columnar section showing the P–Tr succession exposed in the Dayulin section. (B) Logged section showing stratigraphic distributions of MISSs and facies associations from the upper Sunjiagou Formation and lower Liujiagou Formation. FA = facies association. PSS & MISS = physically sedimentary structures and MISS. Question mark (?) represents dubious structures.

Liujiagou and Heshanggou Formations, respectively (Yang et al., 1979; Lin and Fu, 1992; Wang, 1997; Liu and He, 2000; Yuan et al., 2003).

In Dayulin, MISSs occur sporadically in the upper Sunjiagou Formation and are extremely abundant in the lower Liujiagou Formation, ranging a stratal interval of ~100 m in thickness (Fig. 2). Thus, most of the Dayulin MISSs are Induan in age.

3. Material and methods

In Dayulin, abundant MISSs are preserved in muddy siltstone and sandstone from the upper Sunjiagou Formation and lower Liujiagou Formation. All MISSs were measured and photographed in the field. Some well-preserved samples were collected and cut perpendicularly

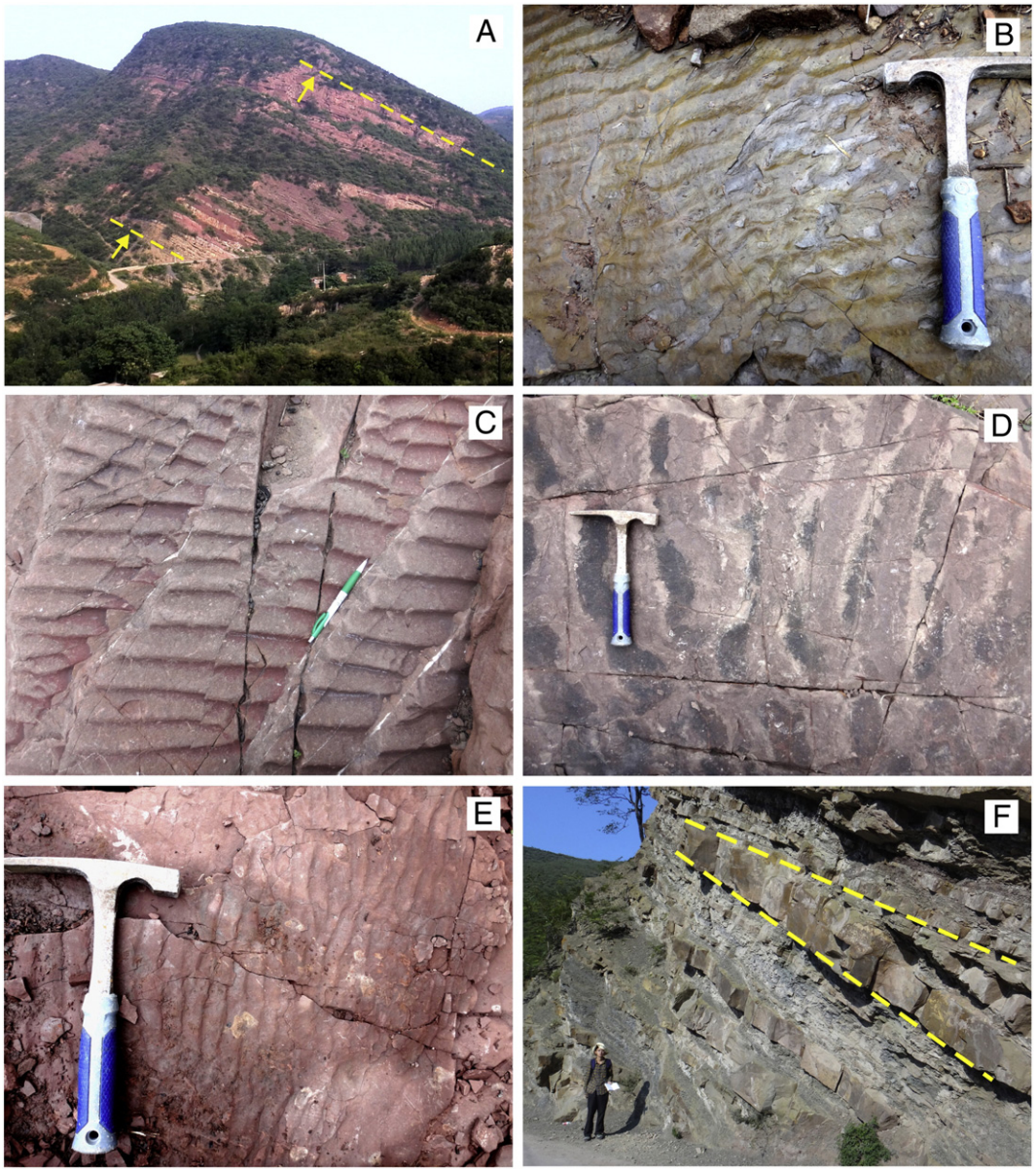

Fig. 3. (A) Field photo showing the Dayulin section (arrows). (B) Asymmetrical, slightly catenary wave-ripples with rounded troughs. Some crests bifurcate and rejoin to produce latticed nests. RI (ripple index) = 9, RSI (ripple symmetrical index) = 1.5. (C–D) Wave-ripple marks characterized by asymmetrical, straight to slightly catenary crests separated by flat troughs. Some crests bifurcate as a result of modification of original wave ripples. RI = 12, RSI = 1.4. (E) Wave-ripple marks featured by straight to slightly catenary crests with wide and rounded troughs. Divergence of crests sometimes occurred. RI = 9, RSI = 3.3. (F) Wedge-shaped sandstone.

to bedding plane surface, and then polished. In order to examine the fossilized microbial remains and grain size variations, the polished surfaces were observed under the LEICA M205 A stereoscope. Thin sections were also made and observed under LEICA DM4500 P microscope equipped with high resolution camera using transmitted light.

A SU8010 FESEM equipped with EDS was also employed to observe fossilized microbial remains and associated secondary minerals in a micron scale. EDS was applied to diagnose mineral composition of MISSs, dubious structures and hosting rocks in order to avoid microbial artifacts due to certain impurities and other modern pollutants. Quartz grains are usually cemented by calcite in siliciclastic sediments which may be corroded. The etching artifacts possibly occur with the increase of the acid strength and etching duration (Kirkland et al., 1999). Thus, acid was not used to clean samples. Instead, the sample was washed in distilled water to clear away pollutants attached to the surfaces. In addition, all samples were coated by gold prior to SEM imaging and EDS analysis. All of the LEICA stereoscope, microscope, and EDS equipped-SEM are equipped at the State Key Laboratory of Biogeology and Environmental Geology, China University of Geosciences (Wuhan).

4. Facies analysis

A combination of physical sedimentary features including bedding surface morphology, sediment texture, composition assemblage, and cross-bedding types (Walker and James, 1992) allows recognition of a total of seven facies types from the MISS-bearing strata. Major characteristics of these seven facies are tabulated here (Table 1). These facies are categorized into three facies associations (FA) in view of their lithofacies features and stratigraphic positions.

Table 1
Sedimentary facies recognized from the MISS-bearing strata in the Dayulin section. RI = Ripple Index; RSI = Ripple Symmetry Index.

Lithofacies	Description	Bed thickness	MISS	Interpretation of sedimentary process
Conglomerate (C)	Gray or reddish conglomerate, sharp scoured base. Gravels are rounded (0.5–2 cm) to subrounded (0.2 × 0.8–1 × 5 cm), usually moderately sorted, and darker than matrix which comprises by calcareous and/or clay minerals	Medium to thickly bedded (0.2–0.8 m)		Upper flow regime generated by riverbed currents which result in the transportation of fine grains, thus, gravels are left behind.
Cross-bedded coarse sandstone (Scc)	Gray or dark gray coarse sandstone bearing well preserved, various types of cross-bedding (i.e., tabular, wedge and trough cross-bedding). Set is 10–30 cm high. Individual cross bed is 1–2 cm thick, and the foresets usually dip at an angle of 20–30°. Paleocurrent direction is northeast	Thickly to very thickly bedded (0.5–2 m)	Polygonal sand cracks	Upper flow regime generated by migration of ripples
Ripple marked coarse sandstone (Src)	Reddish or purple coarse sandstone. Wave dominated-ripple marks are present on the surface of some beds which are asymmetrical (wavelengths 3.5–8 cm and wave heights 3–5 mm; RI = 12; RSI = 1.4), usually bearing straight to slightly catenary crests separated by flat troughs. Some crests bifurcate. Troughs are generally covered by reddish or dark thin muddy layers, indicating the growth and leveling of microbial mats on ripple marks, termed "laminated leveling structure"	Thinly bedded (0.05–0.1 m)	Laminated leveling structures Polygonal sand cracks Worm-like structures	Upper flow regime generated by fluvial waves
Ripple marked medium sandstone (Srm)	Yellow brownish medium sandstone. Asymmetrical (wavelengths 3–4 cm and wave heights 3–5 mm; RI = 9; RSI = 1.5), slightly catenary crested ripple marks are present. Crests are separated by rounded troughs, and some bifurcate and rejoin to produce latticed nests, obviously distinguished from the ripple marks generated by currents	Thinly to medium bedded (0.01–0.015 m)	Laminated leveling structures Polygonal sand cracks	Middle flow regime generated by waves
Fine sandstone (Sf)	Purple or gray yellow, and well sorted fine sandstone. Sharp top and gradual base, usually associated with mudstone	Medium bedded (0.1–0.2 m)	Sponge pore fabrics	Lower flow regime dominated conditions
Ripple marked fine sandstone (Srf)	Claret-colored and well sorted fine sandstone. Sharp top and base. Asymmetrical (wavelengths 1.5–3 cm and wave heights 2–3 mm; RI = 9; RSI = 3.3), straight to slightly catenary crested ripple marks are present. Crests are separated by wide and rounded troughs. Bifurcation of crests sometimes occurs	Thinly bedded (0.01–0.05 m)	Wrinkle structures Laminated leveling structures	Lower flow regime generated by waves
Mudstone (M)	Claret-colored, tabular units, and usually broken fragments due to strong weathering	Medium to thickly bedded (0.4–0.6 m)		Very low energy suspension setting of mud

4.1. Facies association 1 (FA 1)

FA 1 is characterized by ripple-marked medium sandstone (Srm) at its base followed by mudstone (M) with interbeds of fine sandstone (Sf) and two thin conglomerate layers (C). The middle and upper parts of FA 1 stratal interval are composed mainly of M (25 m thick in total) with several thin layers (typically 0.5 m thick in each) of Sf. Asymmetrical, slightly catenary wave-ripple marks (Fig. 3B) with rounded troughs mark the base of FA 1. Some crests bifurcate and rejoin to produce latticed nests. No desiccation cracks are present.

4.2. Facies association 2 (FA 2)

FA 2 shows a fining-up package consisting of thinly-bedded conglomerate (C) (typically 0.1–0.5 m thick) followed by thick cross-stratified coarse sandstone (Scc) and ripple-marked coarse sandstone (Src) (up to 2–8 m thick). The former unit usually bears a sharply scoured base. Gravels are commonly present, rounded to subrounded in outline, and usually moderately sorted (Fig. 4A–C). The latter unit is characterized by large-scale, various types of cross-beddings (i.e. tabular, wedge and trough cross-beddings) whose foresets dip at an angle of 20–30° (Fig. 4D–F) and wave dominated-ripple marks on bedding plane. Tabular cross-beddings in Scc are in sets of 0.1–0.3 m thickness. Individual stratified beds are 1–2 cm thick. The ripple marks are asymmetrical, characterized by straight to slightly catenary crests separated by flat troughs. Some crests bifurcate as a result of modification of original wave ripples (Fig. 3C–D). The sediments of FA 2 are generally coarser than those of FA 1 and FA 3 (see below).

4.3. Facies association 3 (FA 3)

FA 3 is characterized by cyclic fining-up packages. A single package is composed of fine sandstone (Sf) or ripple-stratified fine sandstone (Srf) followed by thick-bedded mudstone (M), 0.5–1.2 m in thickness. When compared with FA 1 and FA 2, FA 3 is characterized by thinly bedded sediments. Sandstone beds are usually thicker than mudstone beds. Asymmetrical, straight to slightly catenary crested ripple marks are commonly present on bedding surface of Srf at the lower part of FA 3. Ripple crests divergence occasionally and are separated by broad, rounded troughs (Fig. 3E).

4.4. Paleoenvironmental interpretation

FA 1 is dominated by thick mudstone with several thin layers of fine- to medium-grained sandstones and conglomerates. The thick package of mudstone indicates sedimentation of fine sediments in a very low energy suspension setting. The absence of desiccation muddy crack possibly indicates a subaquatic setting where sediment was never exposed for a long time. The thin layers of sandstone/conglomerate probably represent periodic and transitory high energy regime. Of these, sandstone layers thicken laterally and appear to be wedge-shaped (Fig. 3F), characteristics of prodelta/delta front setting within a large inland lake. The asymmetrical, slightly

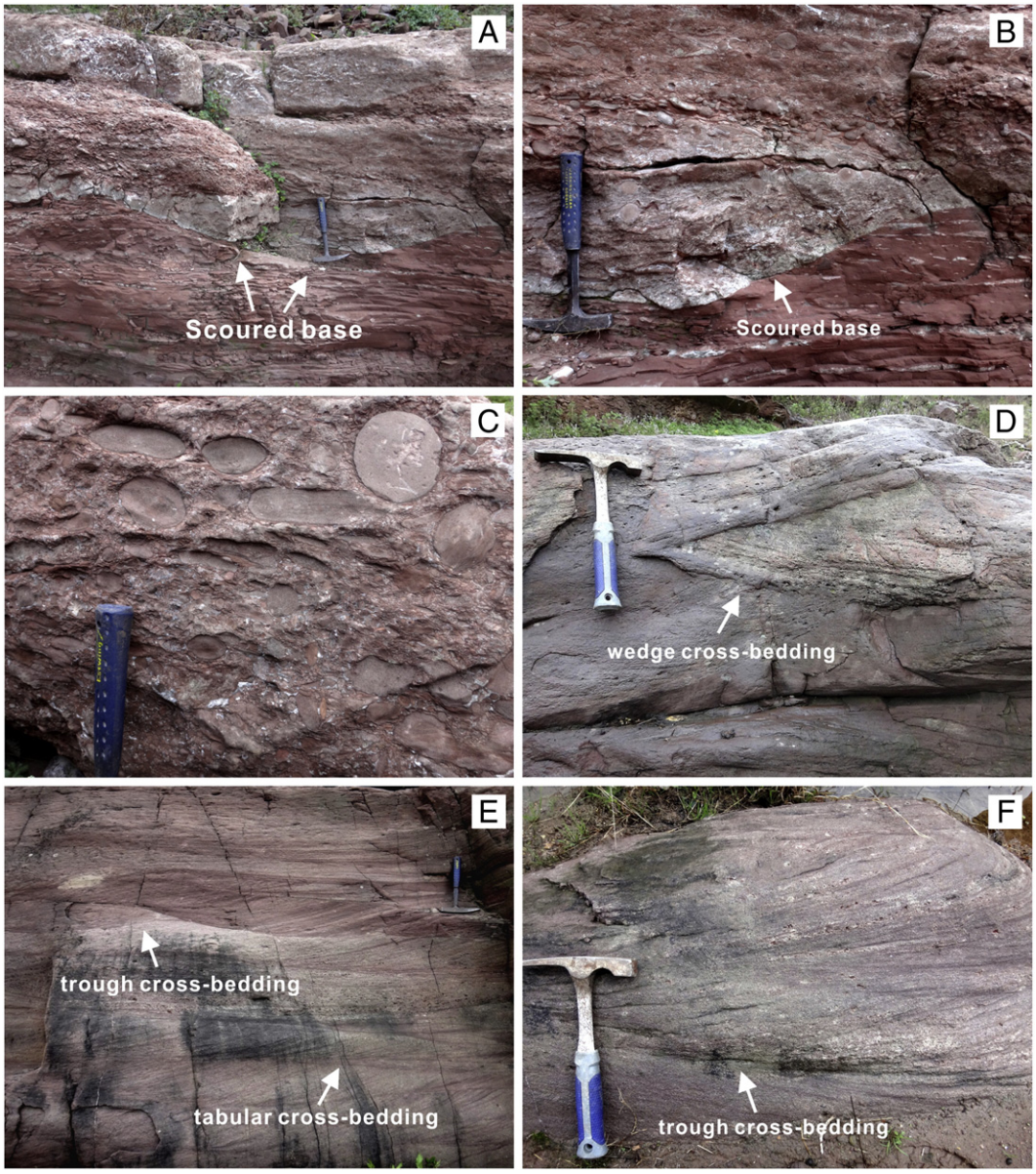

Fig. 4. (A) Field photo showing sharp scoured bases (white arrows) of conglomerates from the Liujiagou Formation. (B) Close-up of (A) showing sharp scoured base of wedge-shaped conglomerates (arrow). (C) Gravels are rounded to subrounded, usually moderately sorted. (D–F) Various types of cross-beddings (i.e. tabular, wedge and trough cross-bedding) that dip at an angle of 20–30°. Tabular cross-beds are in sets of 0.1–0.3 m thickness and individual bed is 1–2 cm thick.

catenary and bifurcated wave-ripples (Fig. 3B) could be generated as a result of migration of paleowaves at different sites.

The combination of conglomerate and coarse sandstone of FA 2 is typically representative of riverbed and point bar setting in fluvial system. The presence of scoured bases in conglomerate with rounded clasts (Fig. 4A–C) indicates the upper flow regime generated by riverbed currents, which resulted in the erosion of riverbed and transportation of fine sediments. The thick-bedded coarse sandstone (Fig. 4D–F) formed as a result of persistent washing from lake wave currents or migration of paleowaves which resulted in asymmetrical, straight to slightly catenary crested ripple marks with flat troughs (Fig. 3C–D). Large-scale, diversified cross-bedding (i.e. tabular, wedge, and trough cross-beddings) provide more support for point bar setting.

The alternation of thinly bedded fine sandstone and mudstone of FA 3 represents flood plain setting. The relatively thick-bedded mudstone represents generally low energy environment, albeit, occasionally interrupted by small-scale storm currents, which is reflected by the episodic presence of fine sandstone. Asymmetrical ripple marks with broad, rounded troughs (Fig. 3E) were likely formed due to modification by waves.

5. Representative MISSs

A total of six types of MISSs are recognized and their morphologies are described as below.

5.1. Polygonal sand cracks (PSCs)

5.1.1. Description

Typical PSCs are preserved as positive epireliefs on bedding surface of medium- to coarse-grained sandstones from the upper Sunjiagou Formation (Bed 1) and lower Liujiagou Formation (Beds 29, 33, 34) (Figs. 2, 5A–D). The positive epireliefs usually project 0.1–0.5 cm

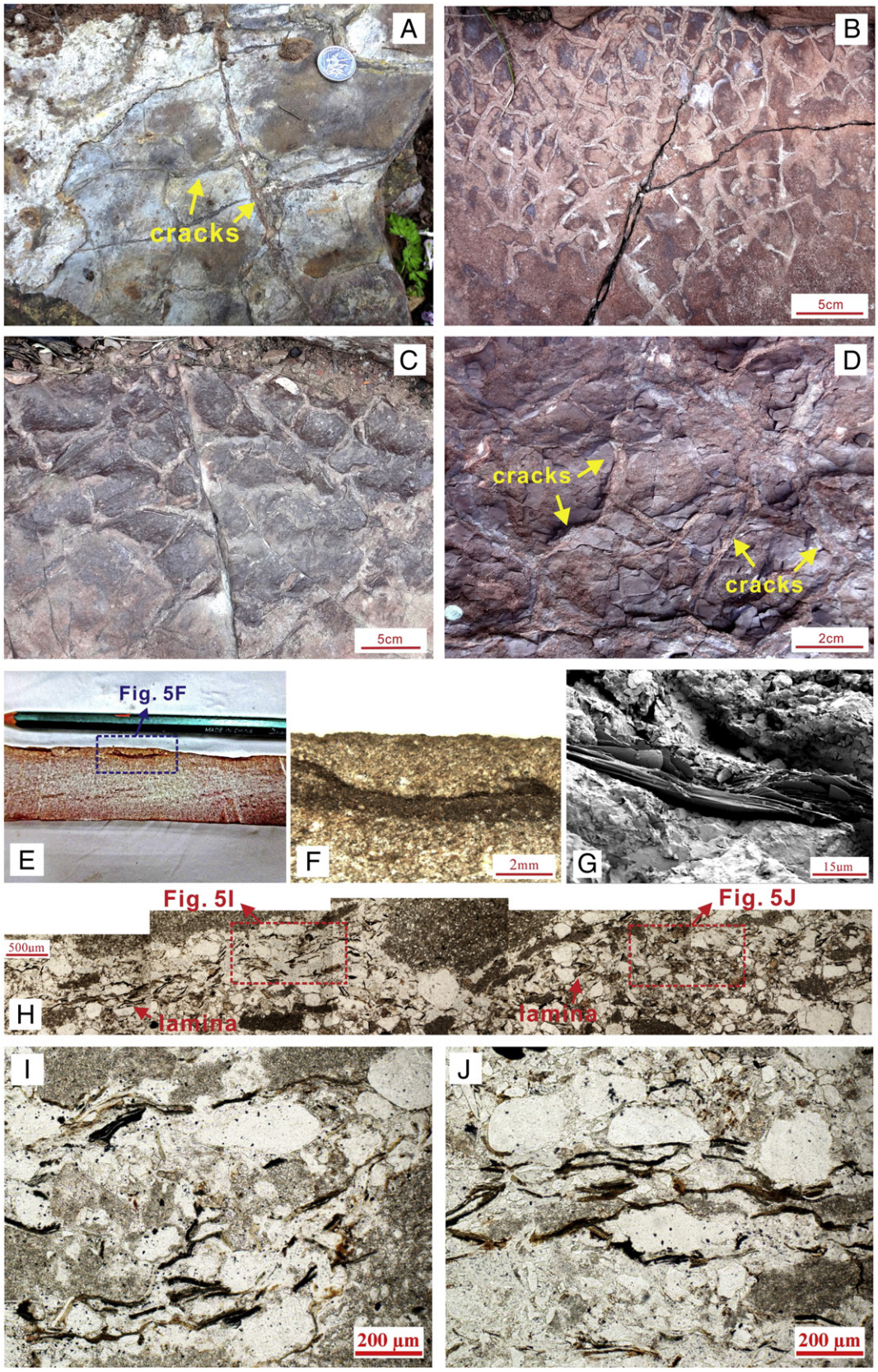

Fig. 5. (A–D) Polygonal sand cracks preserved as epirelief on the bedding plane of sandstone. (E) Polished slab from the Liujiagou Formation (Beds 33 and 34). Note the lamina underneath the 'U'-shaped cracks. (F) Close-ups of (E). (G) SEM images showing sheer clay minerals on the rock surface. (H) Discontinuous filamentous laminae on the uppermost portion of the rock from the Sunjiagou Formation (Bed 1). (I–J) Close-ups of (H) showing dark-colored laminae.

up from bedding plane. Most polygons are tetragonal in geometry; the pentagonal, hexagonal and irregular morphologies also occur occasionally.

PSCs bear a wide range of size variations on various settings. The Sunjiagou cracks are on medium sandstone (i.e., Bed 1). The polygons are relatively large, 6–10 cm long and 4–6 cm wide. Crack width varies from 3 mm to 7 mm, and cracks are usually straight to slightly incurved (Fig. 5A). Their host rocks have relatively fine grains, 0.1–0.5 mm in diameter. In contrast, the Liujiagou cracks (i.e., Beds 33 and 34) outline smaller polygons, which also vary in morphologies on various hosting rocks. These polygons on reddish coarse sandstone (Bed 33) are 1.8–7.0 cm long and 1.0–4.5 cm wide. Cracks are mostly distinct, 3–8 mm in width (Fig. 5B); others are occasionally covered with a very thin dark claret-colored muddy layer (Fig. 5C). Crack polygons on purple-reddish medium to coarse sandstone (Bed 34) are slightly irregular in outline (Fig. 5D).

Polished slab of the Liujiagou PSCs (Beds 33 and 34) shows that dark brownish laminae (1.0–1.5 cm thick) are distinct and beneath the broadly U-shaped cracks, with rather pronounced boundary (Fig. 5E–F). Similar lamination pattern is also pronounced in microphotographs of the Sunjiagou cracks (Bed 1), in which laminae, composed of abundant clay minerals (Fig. 5G), are aligned parallel to bedding plane, and grow occasionally surrounding quartz grains (Fig. 5H–J). EDS analysis suggests that they consist mainly of O, Si and Al, which are overall components of clay minerals, such as illite.

5.1.2. Interpretation

The presence of the U-shaped outline differs clearly from the V-shaped morphology in cross section, indicating that these PSCs are unlikely mud cracks created by desiccation (Allen, 1982). Given that quartz grains are brittle and could migrate to adjust to the optimal location under physical processes, the deformation in pure sandstone is not plausible for the formation of PSCs (Noffke, 2010). Alternatively, the initial growth and colonization on bedding surface can facilitate PSC's development because sticky mucilages secreted by microbes can contribute to the cohesion between siliciclastic detrital grains and microbial mats (Parizot et al., 2005; Sarkar et al., 2006, 2008, 2014; Noffke, 2010). Under the subaerial exposed settings, the secondary desiccation and shrinkage of microbial mass occurred. They might initially form as 'triple junctions' at the early stage (Eriksson et al., 2007) and then resulted in the ultimate features of PSC when quartz particles became loosely distributed (Noffke, 2010; Lan and Chen, 2012; Lan et al., 2013; Banerjee et al., 2014). The microbial carbonaceous remains were left behind in the subsequent processes of decay and decomposition. Then, they were replaced by secondary clay minerals with original morphology retained. This is why clay minerals (i.e., illite) were aligned parallel to one another (Fig. 5G–J).

5.2. Worm-like structures (WLSs)

5.2.1. Description

The WLSs are preserved in situ on bedding plane of sandstone (Beds 20 and 34) of the Liujiagou Formation (Figs. 2, 6A–B). They comprise straight to slightly curved cracks, 5–20 mm long and 1–5 mm wide, which overall resemble worms. Some WLSs are discontinuous and display chaotic-like pattern probably due to strong weathering (Fig. 6A). The host rock is light-gray or reddish fine sandstone, while the bedding surface is covered by a very thin brownish (Fig. 6A) or purple (Fig. 6B) muddy layer. Some dark substances aggregate closely beneath bedding surface. A sharp, winding boundary separating fine, dark sediment from underlying coarser sediment is distinct on polished slab (Fig. 6C).

Under microscope, euhedral mica grains are commonly present in mud-enriched horizon near bedding surface (Fig. 6D) and oriented parallel to bedding plane (Fig. 6E–F). Some quartz particles float in dark laminae (Fig. 6G), which consist mainly of clay minerals (Fig. 6H–J). The quartz grains are 20 μm to 110 μm in diameter, with majority being 30 μm to 60 μm in diameter. The particles embedded in laminae therefore are much finer than those from non-laminated horizons. The latter are mostly 90–180 μm in diameter (Fig. 6G).

5.2.2. Interpretation

As two primary components in physically deposited non-cohesive sand beds, both clay matrix and microbial mats can dehydrate and shrink upon exposure, consequently, sand cracks are created (Schieber, 2004). However, the mud-rich layer on bedding surface is locally distributed and thin, and thus less likely to result in worm-like structures due to a dewatering process. Alternately, like polygonal sand crack analogues, WLSs may be produced due to dehydration of overlying microbial mats, and the mud-rich layer may represent former microbial mats which were replaced by clay minerals. When depositional energy abated, indicated by the deposition of fine sediments (i.e., siltstone), microbial mats colonized and trapped some quartz detritus, which were pushed upward and separated by constantly growing biofilm envelopes (Noffke et al., 2008; Noffke, 2010). Accordingly, the original grain-supporting texture disappeared. In contrast, floating texture within mud-enriched horizon (i.e. probably represents mat fabrics) characterizes rock petrography (Fig. 6G). The euhedral, filamentous mica grains (see Fig. 6F) are possibly aggregated through the processes of baffling, trapping and binding (Noffke et al., 2003b) by the mediation of microbial mass, and that is the reason why they are all oriented parallel to bedding plane (Fig. 6E–F).

5.3. Wrinkle structures (WSs)

5.3.1. Description

WSs are characterized by abundant bulges and pits (or crests and valleys) of irregular directions which can be categorized into 'transparent wrinkle structures' (sensu Noffke et al., 2002). They are well exposed over an area of 20 cm^2 on a bedding plane of fine sandstone of the lower Liujiagou Formation (Figs. 2, 7A–B). The bulges are 3–6 mm long and 2–3 mm high, and the bulge-to-bulge distance ranges from 2 mm to 5 mm. The pits are sealed with gray matrix (i.e. mica grains) and distinguished from adjacent claret-colored bulges (Fig. 7A–B). The host rock possesses quartz grains ranging from 0.025 mm to 0.15 mm in diameter. Intriguingly, straight to slightly incurved, crested ripple marks [1.4–2.7 cm in wavelength and 2–3 mm in waveheight; Ripple Index (RI) = 8; Ripple Symmetry Index (RSI) = 3.2] with broad flattened troughs also occur on wrinkled surfaces (Fig. 7A).

The alternation of elevations and depressions is present on the polished slab cut perpendicular to bedding plane (Fig. 7E). Microphotography suggests that the wrinkled surface is marked by dark, discontinuous and sub-parallel oriented laminae (Fig. 7C), which are composed mainly of clay minerals (Fig. 7D).

5.3.2. Interpretation

Wrinkle structures have been frequently described from shallow marine settings in Precambrian times and aftermaths of major Phanerozoic biocrises (Hagadorn and Bottjer, 1997; Bouougri and Porada, 2002; Pruss et al., 2004, 2006; Sarkar et al., 2004; Banerjee and Jeevankumar, 2005; Mata and Bottjer, 2009a; Banerjee et al., 2010, 2014; Lan et al., 2013; Sakar et al., 2014), but were rarely reported from terrestrial settings (but see Chu et al., 2015). Wrinkle structures remained rather conservative in the geological past and only occurred in two environmental settings: storm-dominated subtidal and intertidal zones (Mata and Bottjer, 2009b). They are usually categorized into two types: 'elephant skin' texture and 'Kinneyia' structures (Porada and Bouougri, 2007). Chu et al. (2015) documented for the first time wrinkle structures from terrestrial settings and considered that these terrestrial WSs share a similar genesis with their counterparts from marine settings in view of their similar morphology. These Dayulin wrinkles resemble Kinneyia in almost all aspects observed, with mm-scale flat-topped, winding bulges, and intervening troughs.

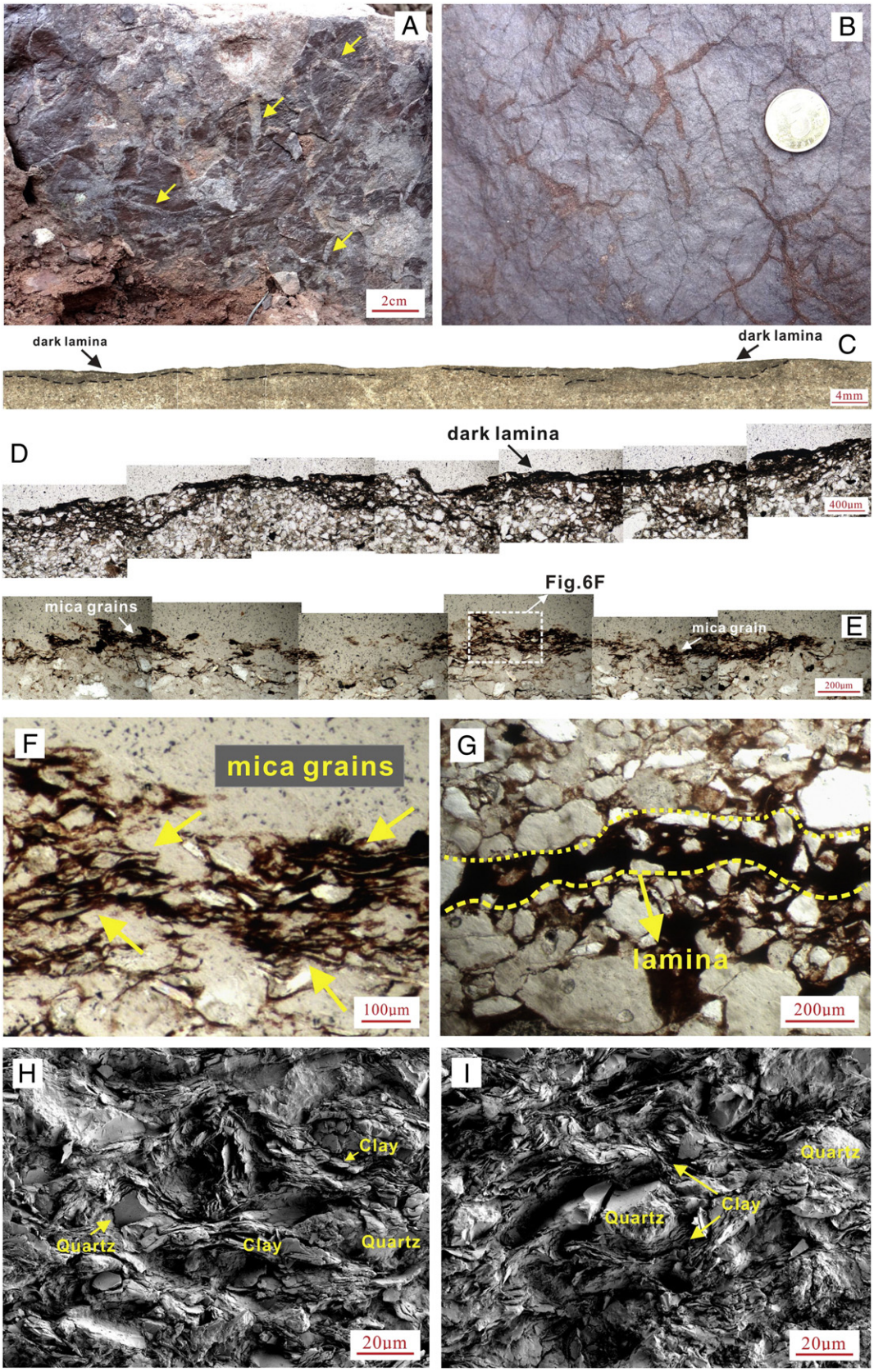

Fig. 6. (A–B) Field photos showing worm-like, straight to slightly curved structures (yellow arrows). Some display chaotic-like pattern due to strong weathering. (C) Very thin, dark and discrete layers on the bedding surface (Bed 20 in Fig. 6A). (D–E) Mud-rich laminae in the upper portion of microphotography and a large amount of euhedral mica grains oriented parallel to bedding plane within mud-enriched horizon of the rock. (F) Close-up of boxed area in E showing mica particles (yellow arrows). (G) Quartz particles within laminae (within two dash lines; yellow arrow) are much finer than those from non-laminated horizons. (H–I) SEM photography suggests that dark laminae consist mainly of clay minerals.

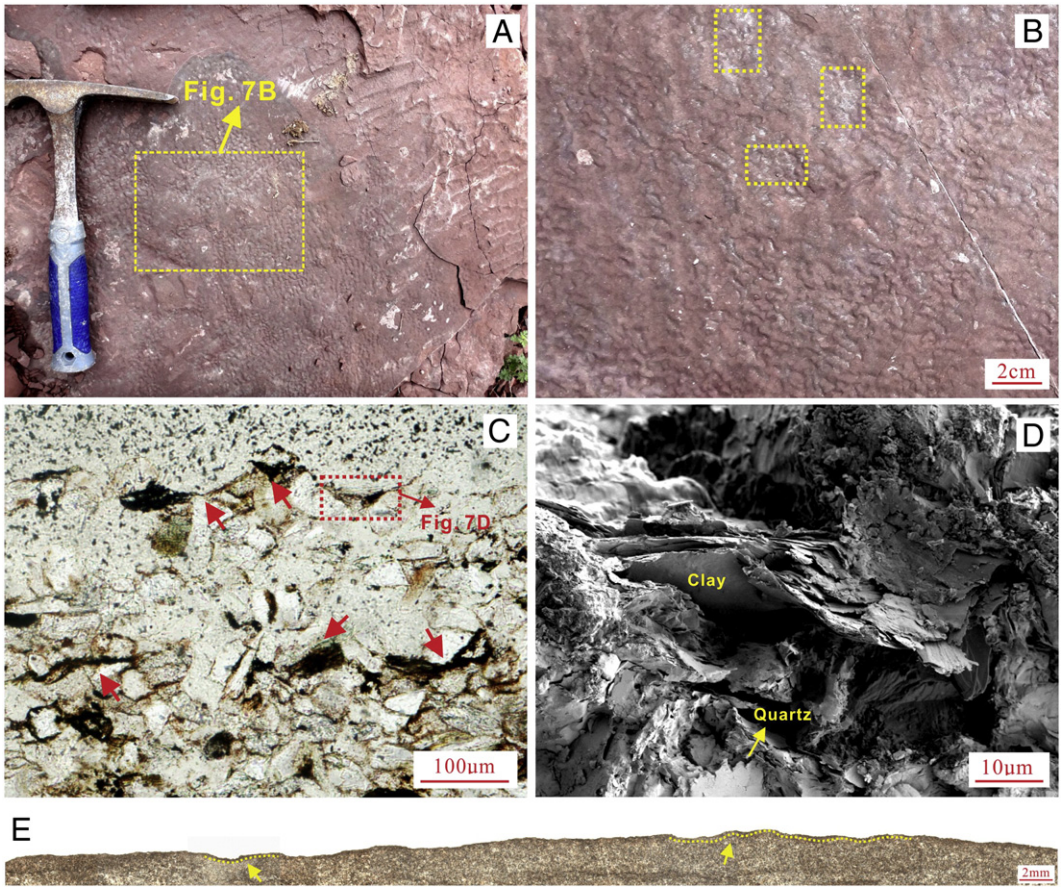

Fig. 7. (A) Field photos showing wrinkle structures preserved on surface of sandstone. (B) Close-up of boxed area in A showing pronounced wrinkled surfaces with pronounced mica particles within yellow dash line boxes. (C) Dark, discontinuous and sub-parallel oriented filaments on the uppermost portion of microphotography. (D) SEM images suggest that laminae in boxed area in C are composed of clay minerals. (E) Alternation of elevations and depressions shown by polished slab cut perpendicular to the bedding plane.

Some miniature load structures are believed to be purely physically induced small-scale wrinkly structures. They are confused with microbially mediated 'wrinkle structures' (Porada and Bouougri, 2007). The Dayulin structures, however, less likely resulted in load forces due to lack of underlying mudstone/argillite beneath the wrinkled surface. The latter is crucial in producing load structures (Porada and Bouougri, 2007). In Dayulin, the Kinneyia troughs are overlain by abundant mica and very thin claret-colored muddy layers (Fig. 7A–B), which were thought to be related to the baffling, trapping and binding of primitive microbial mass (Bouougri and Porada, 2002; Noffke et al., 2002, 2003b). The presence of discontinuous, parallel-aligned laminae observed under the microscope (Fig. 7C) provides more support for the biogenicity of wrinkle structures. More recently, Mariotti et al. (2014) observed the formation process of modern wrinkled mats and detected that the pits formed when porous mat aggregates anchored to the bed, then oscillated, scoured the sand, and then bulges formed under the transportation of sand grains from depressions to bumps with the oscillatory rolling, dragging and hopping of rounded mat fragments.

5.4. Sponge pore fabrics (SPFs)

5.4.1. Description

SPFs are preserved on bedding surface of light purple fine sandstone of the lower Liujiagou Formation (Figs. 2, 8A–B). Single SPFs are rounded to subrounded (occasionally irregular) pores, 0.2–1.0 cm in diameter, which are randomly arranged. These pores are filled with sparitic calcite, and thus exhibit light color in the field.

Polished slab and thin section cut perpendicular to bedding plane show that a very thin layer of relatively dark matrix covers the rock surface (Fig. 8C–D), which contains abundant fibrous mica grains oriented parallel to bedding plane (Fig. 8E–F). The mica particles are usually aligned along the margin of quartz particles, typical of euhedral morphology (Fig. 8E), implying that they are not of secondary minerals. Of particular interest is that quartz detritus vary in sizes (Fig. 9A). Quartz grains trapped within laminae (dark layers) are 20–100 μm long, with majority ranging from 30–60 μm in length. They are readily different from those embedded in non-laminated horizons (light-colored layers), which are 50–300 μm long with majority being 80–180 μm long (Fig. 9A). SEM imaging also indicates that the aggregated and veneer-like clay minerals are present on bedding surface, with the alignment of parallel to subparallel orientation (Fig. 9B–C).

5.4.2. Interpretation

Given their occurrence in sandstone, the SPFs cannot be treated as the 'bird-eye' structure of pertidal carbonate setting. Accordingly, the sponge (porosity) pore fabrics likely formed with the influence of overlying microbial organics, as in the vesicular structure of desert soils (McFadden et al., 1998). Like a sealing carpet, microbial mat would block the escape of gas that was generated during microbial metabolic or subsequent decomposition processes. The pores formed under the pressure of increasingly accumulated gas (Noffke, 2010). When microbes gradually decayed, the gas bubbles were filled with calcite. The primitive morphological features of microbial aggregates were usually remained during the replacement. The enrichment of euhedral mica grains and their parallel alignment imply that they were likely trapped and aggregated by the 'flypaper' effect with the involvement of

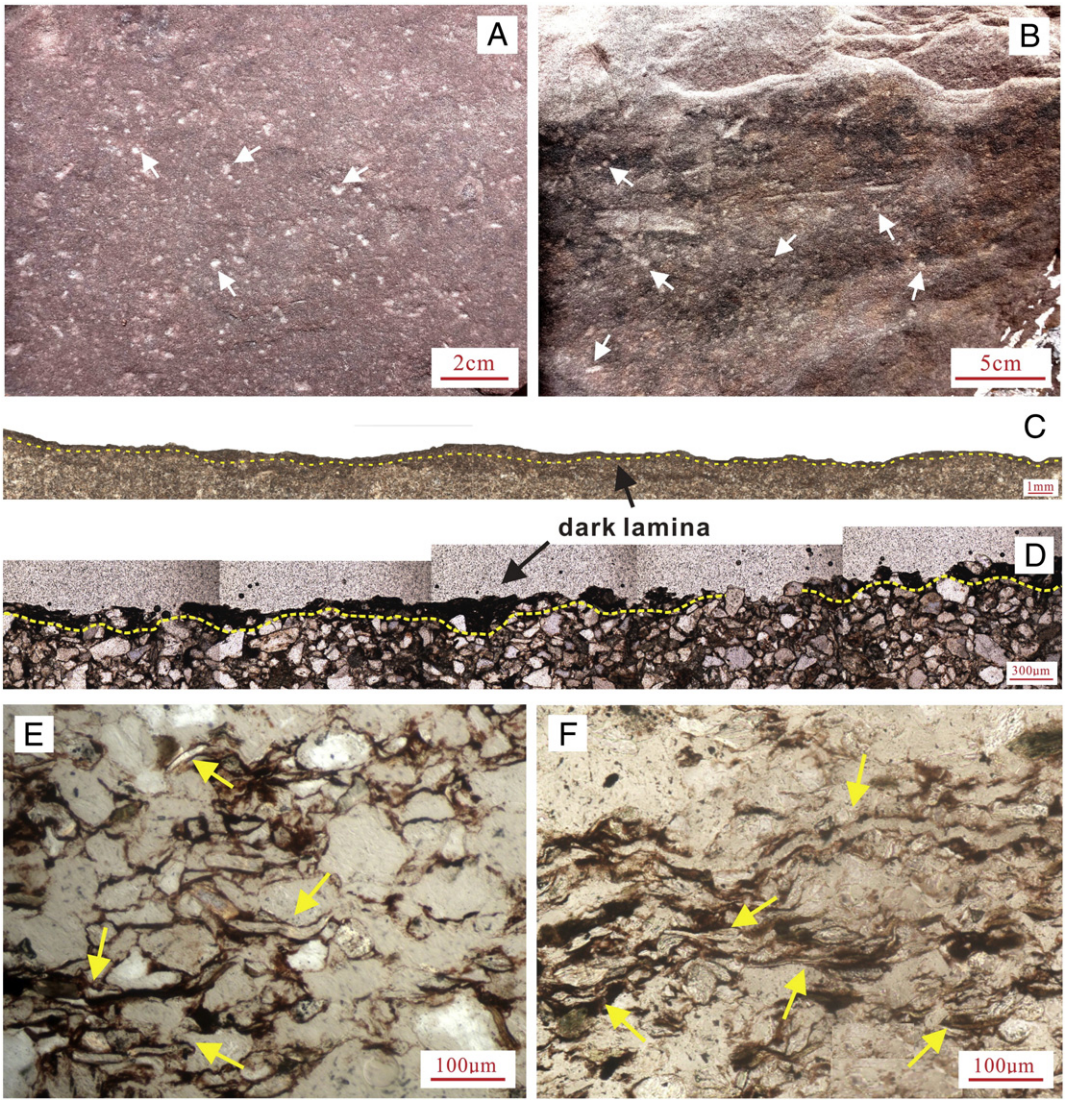

Fig. 8. (A–B) Field photos showing sponge pore fabrics on bedding surface and vertical cross-section (arrows), respectively. White, round to subrounded (some are irregular) pores seem to be arranged randomly, filled with carbonate-minerals (i.e. sparite). (C–D) A dark thin muddy layer on rock surface shown by polished slab and thin section cut perpendicular to bedding plane, respectively. (E–F) Abundant mica grains (arrows) oriented parallel to bedding surface.

microbial organics (Schieber, 1998). The relatively dark-colored laminae under microscope indicate the existence of former microbial mats, because microbes usually colonize in the low-energy settings in which the suspending fine grains would gradually accumulate under the baffling, trapping and binding of the organisms (Noffke et al., 2003b; Noffke, 2009, 2010). The sponge pores were filled with sparitic calcite during the diagenesis. Similar structures are also commonly present in shallow marine sandstones of late Neoproterozoic age in the Kimberley region, northwest Australia, although the latter are associated with erosional remnants and pockets (Lan and Chen, 2013).

5.5. Gas domes (GDs)

5.5.1. Description

GDs occur on bedding planes of coarse sandstone (Bed 13) in the lower Liujiagou Formation (Fig. 2), characterized by hemispherical or subrounded domes. Most domes show a distinct positive relief on bedding plane, although some have very low reliefs (Fig. 10B). Single GDs comprise light gray infillings and dark peripheral components (Fig. 10A–B). They vary in size, with inner core being 1.5–9.5 cm and outer wall being 17–25 cm in diameter, respectively. Moreover, some GDs are characterized by the deformed, irregular outer walls and former inner core (Fig. 10C–D). Grain sizes of the host rock are indistinguishable from that of domal structures. All gas domes are randomly distributed without aggregations.

5.5.2. Interpretation

The elevated morphology and uniform quartz size of gas domes are not in accordance with the dewatering structures, which generally occur in fine- to medium-grained laminated units (Lowe, 1975; Mazzoli and Carnemolla, 1993). They appear as protuberances or small pillars bounded by downwards-warping laminations due to weathering (Owen, 1996; Frey et al., 2009). The homogeneous grain composition indicates GDs cannot be misinterpreted as compaction folding, which formed due to differential reaction to load controlled compaction during diagenesis (Davies, 1984). Therefore, the domal structures formed likely with involvement of microbial activities, albeit, the role played by diagenesis may not be completely ruled out.

Modern analogy of GDs is commonly present in peritidal settings and often associated with epibenthic microbial mats that sealed underlying sediments. The domal size correlates well with the thickness of microbial mats (Bose and Chafetz, 2009; Sakar et al., 2014). Thus,

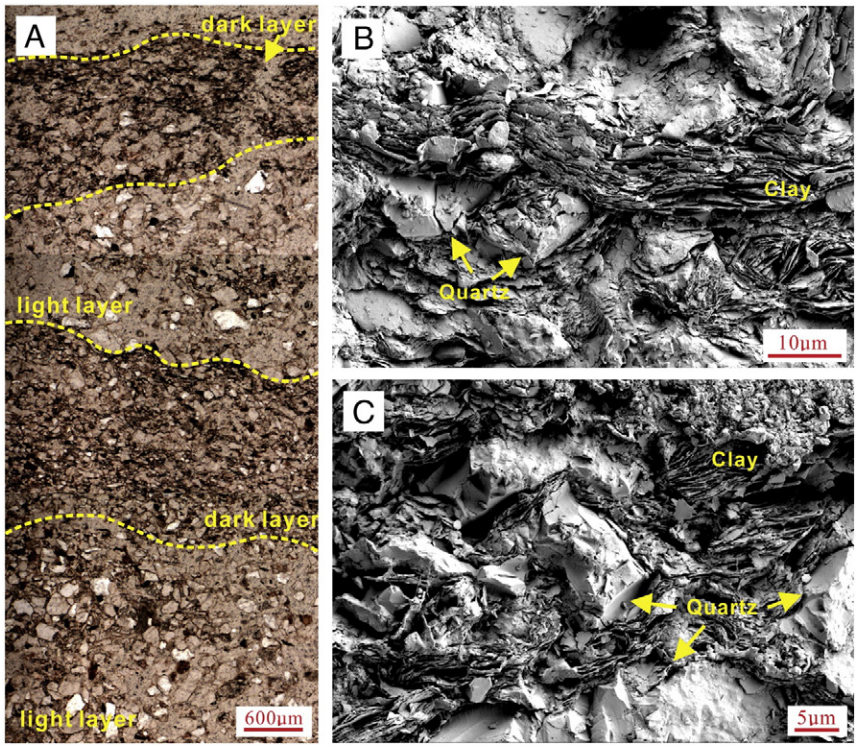

Fig. 9. (A) Small quartz detritus concentrating in laminated layers within thin section perpendicular to bedding plane, showing distinct pattern of alternating light-colored layers and dark-colored layers. (B–C) SEM photography showing aggregated and veneer-like clay minerals on bedding surface, with alignment of parallel to subparallel orientation. Note some quartz grains are surrounded by clay minerals.

these large DYL domal structures might have formed in association with thick microbial mats. Gas accumulated in microbial metabolic and decay processes due to prohibition of viscous microbial organics, during which microbial mats were lifted due to elevating gas pressure, losing contact with its underlying substrate (Bottjer and Hagadorn, 2007; Noffke, 2010; Lan and Chen, 2012, 2013). Meanwhile, the sediments would have been carried from the base to top within the dome by upward migration of gases (Lan and Chen, 2012) and suspending fine quartz grains might accumulate on the top under the processes of biofilm baffling, trapping and binding (Noffke et al., 2003b; Noffke, 2009, 2010). Thus, the inner core of the DYL domal structures show a light color probably due to pure sands in contrast with the relatively dark outer wall,

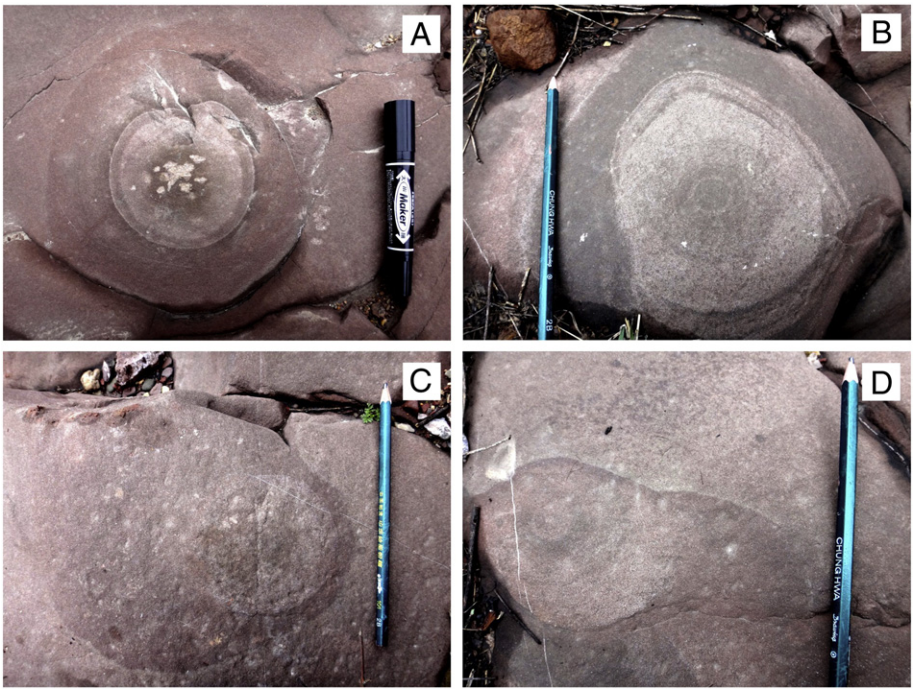

Fig. 10. (A) Field photos showing domal structures, with light gray infillings enclosed by a dark gray wall. (B) No elevation of gas dome projecting from bedding plane. (C–D) Slightly deformed domal structures showing irregular wall and infillings.

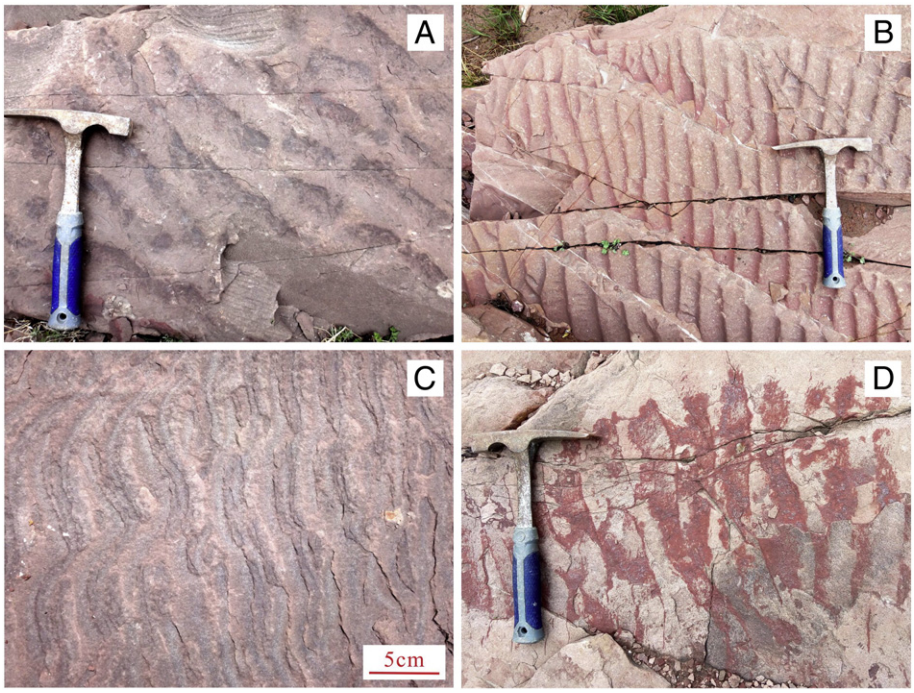

Fig. 11. (A) Ridged and troughed ripple marks, coexisting with small-scale, patchy-like ripple marks on bedding surface. (B) Pronounced ripple marks. (C–D) Weakly ridged ripple marks, which are flattened with troughs being sealed with a thin muddy layer.

which comprises sand-sized quartz with mixture of few organics or secondary clay minerals as the result of decay of the earlier biomass. Some domes lacking protuberances were probably generated by subsequent rupture or compaction during diagenesis. Furthermore, in the wake of occasional hydraulic reworking in flood plain, microbial mats would be deformed, bearing irregular outer walls. These enigmatic structures also resemble the disc-shaped "discoidal microbial colony" reported from the Precambrian Vindhyan Supergroup and Jodhpur Group (Banerjee et al., 2010, 2014) and modern environments (Banerjee, 2012; Sakar et al., 2014). However, additional evidence is needed to illuminate the possible relationship between them.

5.6. Leveled ripple marks (LRMs)

5.6.1. Description

LRMs are commonly present on bedding surfaces of medium- to coarse-grained sandstone in the upper Sunjiagou and lower Liujiagou Formations in Dayulin (Fig. 2). They are further categorized into two types: distinctly ridged and troughed and weakly ridged ripple marks. The former exhibit clearly pronounced ripple ridges and troughs (Figs. 3B, 11A–B). Some have ripple lengths of 3–4 cm and heights of 3–5 mm, sealed with a very thin, yellow-colored layer (Bed 1; Fig. 3B). Others have ripple lengths of 3.5–8 cm and heights of 3–5 mm, with the troughs being covered by a thin, dark-colored layer (Bed 11; Fig. 11A). In addition, some small, patchy ripple marks are present on the same bedding surface (Fig. 11A). LRMs also occur in the upper portion of the MISS-bearing strata (Bed 33), featured by flat and broad troughs with sharp ridges (Fig. 11B). In contrast, the weakly ridged ripple marks have rather low ridges and broad troughs. They are rarely present, confined to Beds 13 and 34 (Fig. 11C–D).

Although LRMs vary in morphology and sizes, the troughs of both types of LRMs are sealed with very thin, muddy coatings. They are distinguished from host rock in color. Therefore, they formed unlikely due to weathering formation.

Microscopic and SEM imaging analyses of non-transparent LRMs (Bed 13) show that some laminae are scattered on the surface with their alignment parallel to bedding plane (Fig. 12A–B). Within the host rock typically filamentous mica grains are also scattered between quartz grains (40–140 μm in diameter) and oriented parallel to bedding plane (Fig. 12C–D). The dark laminae are also identified in SEM images and comprise clay minerals (dominated by Al, Si, O elements). They surrounded detrital particles and are also orientated parallel to bedding plane (Fig. 12E–F).

5.6.2. Interpretation

If only taking physical processes into account, the formation of LRMs is enigmatic. Although the reworking by relatively weak wave/current actions has been invoked for formation of LRMs, the presence of very thin muddy layers on all troughs makes it untenable that only physical processes are responsible. Growing evidence shows microbial involvement is crucial in the formation of LRMs (Noffke et al., 2001; Noffke, 2010). Inferred fossilized microbial mats covered the surface of the earlier ripple-marked sediments (reworked by former wave/currents). When covered by relatively thin microbial mats, ripple marks may have been better preserved with elevated ridges and deep troughs. Otherwise, ripple mark crests are flattened into low ridges. Nevertheless, even the non-transparent LRMs can also be recognized after lithification because microbial organics were recorded in the replacement by clay minerals, consisting of the thin muddy coatings in the troughs. The oriented mica grains have been often interpreted as the result of baffling and trapping of microbes (Noffke et al., 2001; Sarkar et al., 2008; Mata and Bottjer, 2009a; Noffke, 2010).

Besides, the co-occurrence of small scale, patchy ripple marks (Bed 11; Fig. 11A) with the typical LRMs indicates that microbial mats are unevenly distributed. These small-scale ripple marks were probably sealed by relatively thin microbial mats, and thus have been more strongly shaped by hydraulic reworking than microbial activities.

5.7. Co-occurrence of various types of MISSs

Two different types of MISS, leveled ripple marks and sand cracks, co-occur on the same bedding plane of the Liujiagou Formation

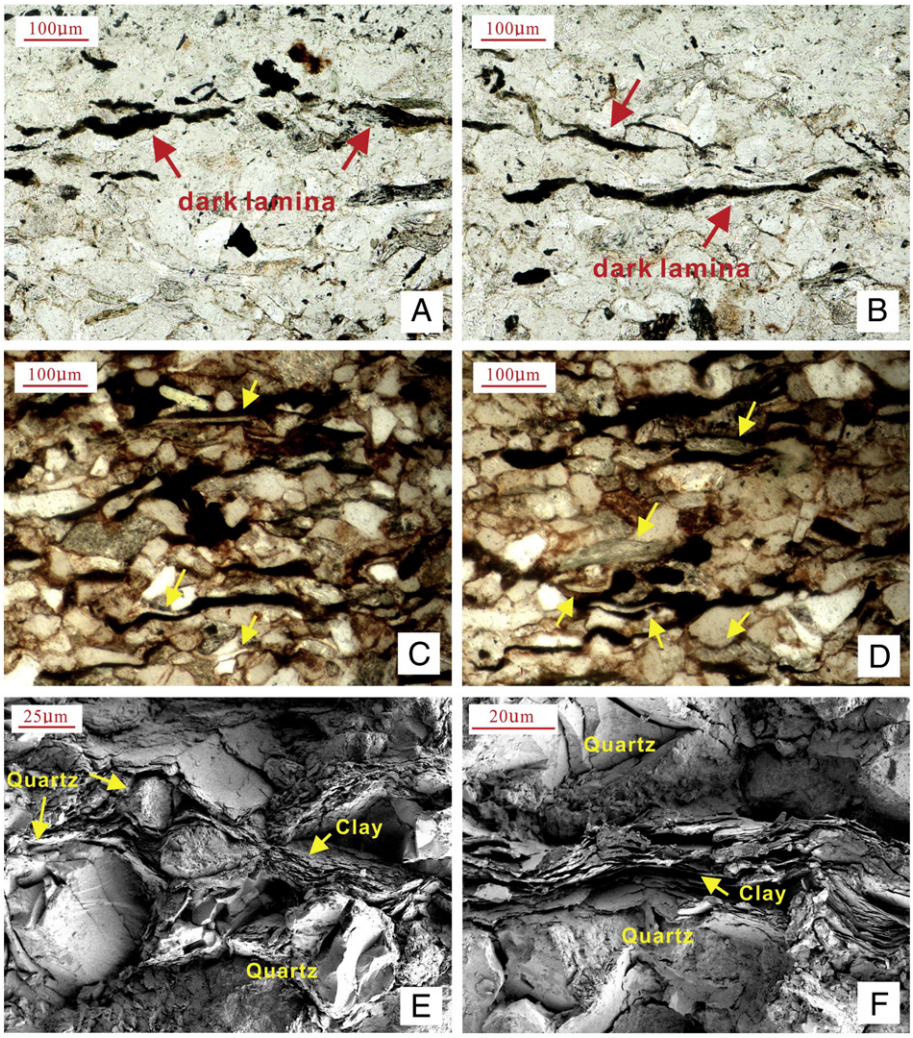

Fig. 12. (A–B) Some dark laminae aligned parallel to bedding plane (arrows). (C–D) Filamentous and parallel-oriented mica particles (white arrows) scattered between quartz grains. (E–F) SEM images show that abundant clay minerals (arrows) occur near bedding plane and are arranged along detrital particles or quartz grains.

(Fig. 2). The associated MISSs are preserved in situ or had been transported.

5.7.1. Description

The in situ associated MISSs occur on bedding plane of light reddish coarse sandstone (Bed 29; Figs. 2, 13A–B); they are covered by a very thin, dark reddish and mud-rich layer on the surface. The ripple marks possess indistinct crests and troughs, which, however, form visible alternating elevations and depressions (Fig. 13A). The associated polygonal cracks are filled with light-colored coarse sandstone, which is indistinguishable from the host rock. Cracks are 9.0–25 cm in length and 3.0–15 mm in width, projecting 1–2 mm into sediments from bedding surface (Fig. 13B). The polygons, generally 21–70 cm long and 8.0–33 cm wide, include tetragonal, pentagonal, hexagonal, and irregular geometries (Fig. 13A).

The transported MISSs vary in morphology (Beds 19 and 28). The one on Bed 19 is well preserved on light reddish coarse sandstone, sealed by a thin, claret-colored, muddy layer on the bedding plane. Rounded crested, asymmetrical ripple marks with flat, wide troughs are present. Their wavelengths vary from 3.5 cm to 6.5 cm and amplitudes have a size range of 1.0–1.5 cm (Fig. 13C). The cracks co-occur on the bed, 0.8–5 cm long and 1–2 mm wide, overlying the ripple marks, whose compositions accord with those of the host rock (Fig. 13C). The other (Bed 28) is similar in terms of the features of host rock and associated ripple marks, while the cracks are clearly different, which display spindle-like, 'V' shaped and triple junction morphology (Fig. 13D). Cracks are 0.9–2.5 cm long and 1–4 mm wide.

Polished slab and corresponding microscope imaging show that one thin, dark mud-rich layer is present on the topmost bedding plane (Fig. 13E–F). The dark lamina consists of a large amount of clay minerals pervasively surrounding quartz grains, illuminated by SEM investigations (Fig. 13G–H). Intriguingly, the other lamina can be recognized within the vertical cross-section, occurring about 1 cm underneath bedding plane (Fig. 14A). Both microscopic and SEM analyses suggest that abundant fiber-like mica grains are interwoven by the relatively thick lamina (Fig. 14B, E), composed mainly of clay minerals (Fig. 14F). The mica grains are aligned parallel or sub-parallel to bedding plane (Fig. 14E), as demonstrated on the rose diagram (Fig. 14B–D). In addition, quartz particles display no grain-to-grain contact, but float with their long axes parallel to sedimentary surface within lamina (Fig. 14B, E–F). These grains are 60–160 μm in diameter, but concentrated on 70–90 μm in size, much finer than those out of the lamina, whose sizes range from 130–250 μm (Fig. 14B).

5.7.2. Interpretation

The dark colored lamina on the bedding plane (Fig. 13E–F) is interpreted as a possible fossilized microbial fabric. These microbial mats covered the ripple-marked sediments and varied in thickness from place to place. The relatively thick lamina indicates that local

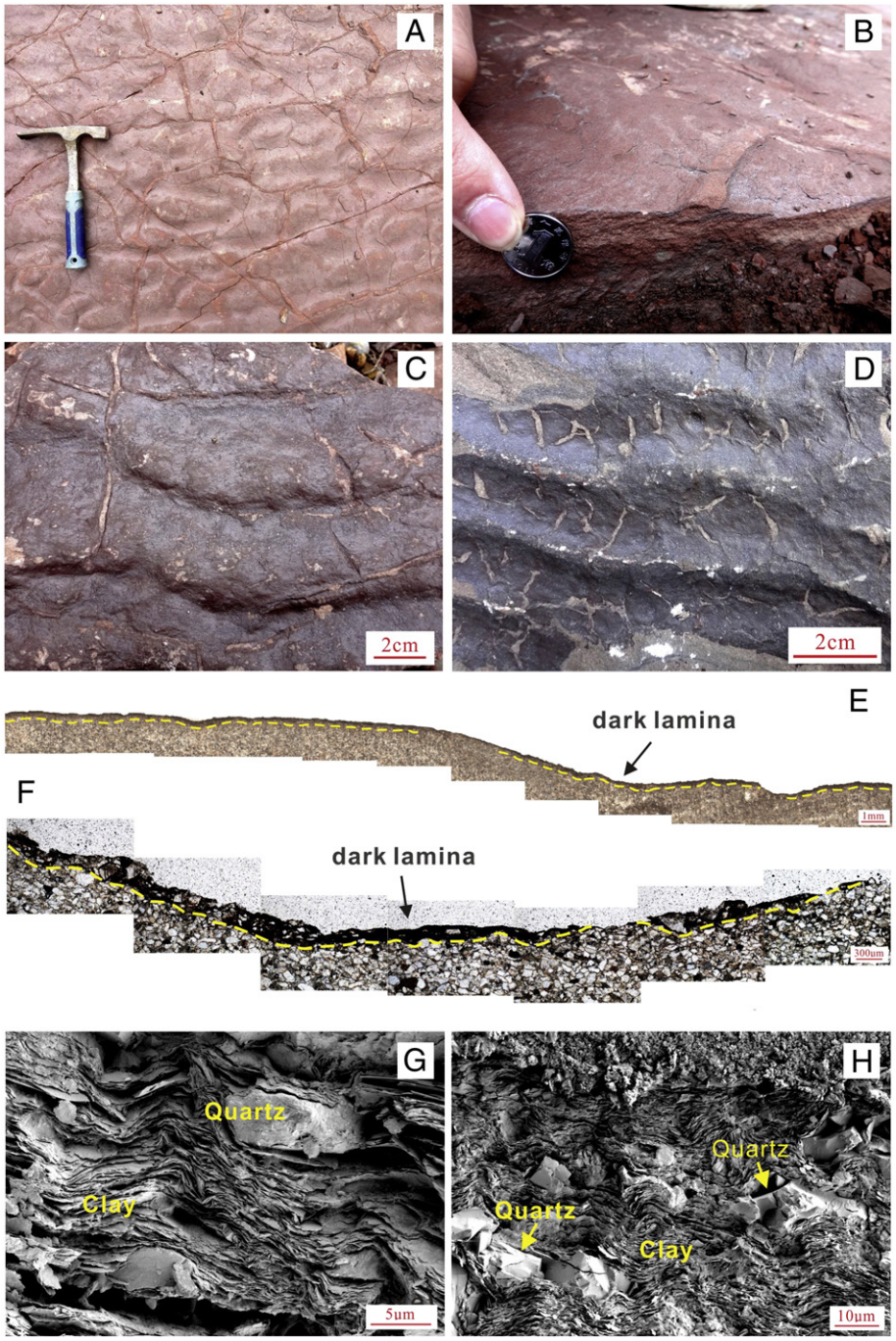

Fig. 13. (A–D) Field photos showing the co-occurrence of leveled ripple marks and sand cracks. The cracks display polygonal (A–B, Bed 29; C, Bed 19) or spindle-like, V-shaped and triple junction morphology (D, Bed 28). (E–F) Thin, dark, mud-rich layer near bedding surface. (G–H) SEM images suggest the uppermost laminae are composed of abundant sheer clay minerals, surrounding the quartz particles, which are aligned parallel to bedding plane.

aquatic or subaerial conditions were stable and favorable for microbial mat's sustained growth. In contrast, when local conditions were inhospitable for microbial mat's growth, fully transparent ripple marks formed, and some of these can be seen on bedding plane (Bed 29). The polygonal sand cracks were created, resulting from dehydration of the locally thick, water-enriched microbial organics. Few organics would remain during the decay of microbial mats over time, but be replaced by a large component of clay minerals (Fig. 13G–H). Interestingly, the lamina below the surface within the vertical cross-section could stand for the earlier colonization and development of biomass. The quartz particles within the lamina (i.e. represent possible mat fabrics) are relatively fine in size (Fig. 14B), because the filaments (i.e. microbes) would create micro-zones of lower current velocity that allows suspended, silt-sized detritus to settle (Noffke, 2010).

6. Discussion

6.1. Biogenicity of the Early Triassic MISS on terrestrial ecosystems

MISS is a useful signature for understanding evolution of microbial ecosystems in geological history by comparing modern analogues (Noffke et al., 1997, 2003b; Noffke, 2010). However, caution is needed

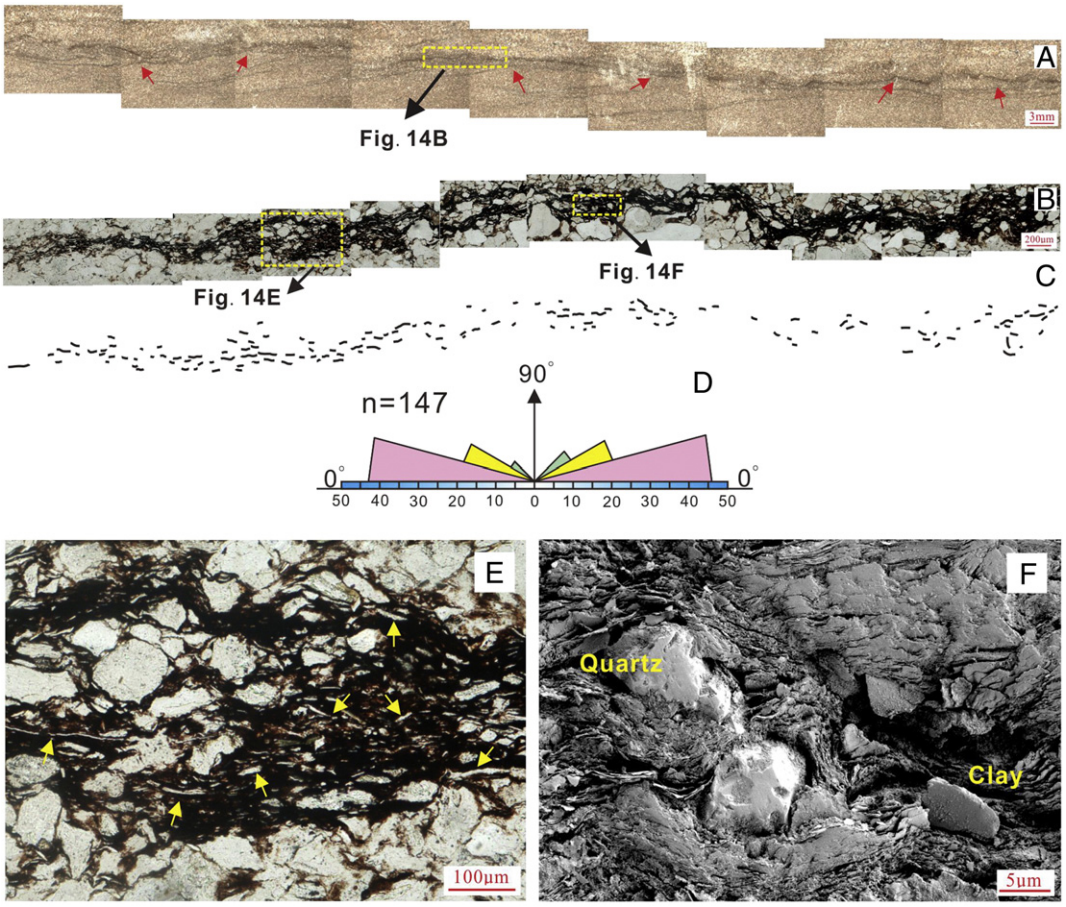

Fig. 14. (A) Laminae recognized within vertical cross-section, occurring about 1 cm underneath bedding surface (Bed 29). (B) Abundant fiber-like mica grains are interwoven by relatively thick laminae and quartz particles display no grain-to-grain contact, but float with their long axes parallel to bedding surface within laminae, further analyzed by SEM imaging (Fig. 14F). (C) Sketches showing orientation of mica grains in Fig. 14B. (D) Rose diagram indicates that mica grains are aligned parallel to sub-parallel to bedding plane. (E) Close-up of boxed area in B showing abundant mica particles within laminae (yellow arrows). (F) SEM image of boxed area in B shows that thin clay minerals surrounding quartz particles.

because some MISS-like structures have geometry and dimensions so similar that they are difficult to distinguish from each other (Noffke, 2009), and from purely physical or chemical processes without involvement of microbes (Schieber et al., 2007).

The Dayulin MISSs are all commonly present in shallow marine siliciclastic settings in the geological past (Noffke et al., 2003a, 2008; Pruss et al., 2004; Porada and Bouougri, 2008; Mata and Bottjer, 2009a,2009b; Lan and Chen, 2012, 2013; Lan et al., 2013). Of these, polygonal sand cracks, worm-like structures, wrinkle structures, and leveled ripple marks are sealed by a very thin, dark mud-rich layer, possibly representing primitive microbial organics. Thin laminae are also commonly present just beneath the bedding plane (Figs. 5H–J, 6D, 7C, 8C–D, 12A–B, 13E–F). Their counterparts occurred frequently in deep time MISSs and have been interpreted as an indirect evidence of ancient biomass arisen from mat-decay products (Garlick, 1988; Schieber, 1999; Sur et al., 2006; Seilacher, 2007; Noffke, 2010; Samanta et al., 2011), composed of a majority of clay minerals (chemically comprise by Al, Si and O). They were created by the replacement of microbial carbonaceous products subsequently in the aftermath of biomass degradation or during early diagenesis, which may have inherited the original morphology of mat-constructing microbes. Mica grains embedded in laminated layers show euhedral and filamentous morphology and are oriented parallel to bedding plane in this study (Figs. 6E–F, 8E–F, 12C–D, 14B, E) and previous literature (e.g., Noffke et al., 2003b; Banerjee and Jeevankumar, 2005; Seilacher, 2007; Noffke, 2010; Luo et al., 2013), indicating that they could not be formed as cement, but formed probably due to 'flypaper effect' with the involvement of biomass (Schieber, 1998). Other MISSs (i.e., gas domes, sponge pore fabrics) resemble superficially their marine counterparts. Growing evidence shows that those marine examples of MISSs are likely biogenetic (Noffke, 2010; Lan and Chen, 2013).

Besides, the oriented grains float commonly within laminae of the Dayulin MISSs (Figs. 6G–I, 9B–C, 12E, 13F, 14B). Modern laboratory experiments show that the mediation of microbial organics has played an important role in the formation of oriented grains. This is because sand particles were pushed upward by constantly growing of biofilm envelopes, finally separated from one another (Noffke, 2010). Quartz grains therefore have floating texture and were oriented in alignment parallel to bedding planes.

To probe genesis of these MISSs, we have also observed several types of sedimentary structures possibly related to biomass in modern fluvial systems (Fig. 15A–D). These enigmatic structures are exposed along the small creek, near the Dayulin section where the creek is a microbe-rich system (Fig. 15E–F) with relatively dry condition. Much evidence shows that microbial activity may have been crucial in the formation of these modern 'MISSs' (i.e., Noffke, 2010), suggesting that their counterparts in geological past may also be likely biogenic in origin.

All lines of evidence suggest that the Dayulin MISSs are of biogenic origin.

6.2. Depositional preference of MISSs in terrestrial ecosystems

Geobiologic analyses on MISS examples from 20 studied sites in modern oceans reveal that microbial mats inhabited a wide range of

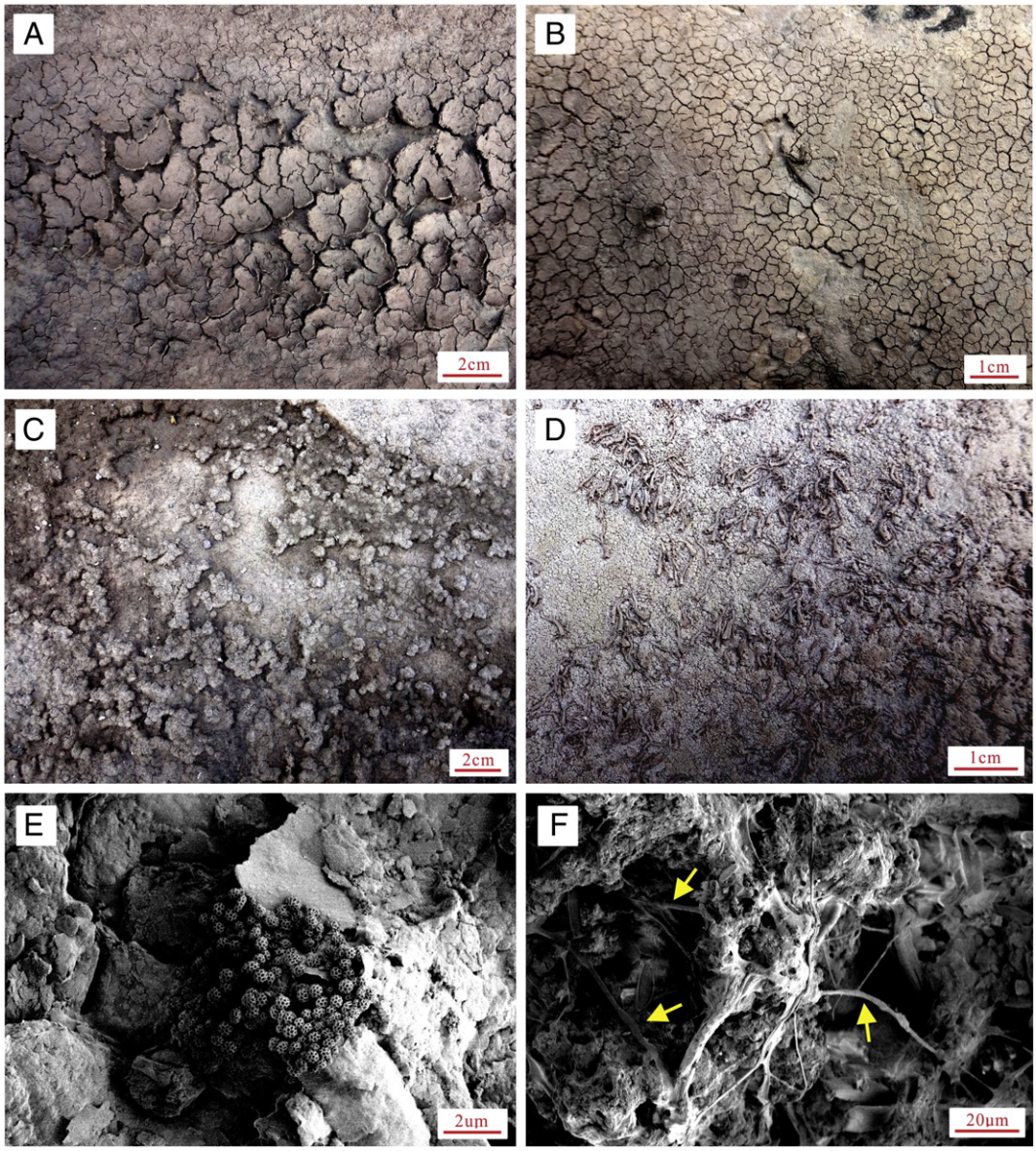

Fig. 15. (A–D) Field photos showing possible modern counterparts of MISSs, which vary in morphology and size from a small creek near the Dayulin section. (E) Microspheroids shown in SEM image. (F) Filaments (yellow arrows) in SEM image.

niches from deep sea to nearshore due to the long-term pattern of storms and tidal cyclicities (Noffke, 2010). Similar pattern is also suggested by the deep time marine MISSs (Bouougri and Porada, 2002; Mata and Bottjer, 2009b; Eriksson et al., 2010; Noffke, 2010; Lan and Chen, 2012, 2013). On land such MISSs are well known back into the Archean (Mossman et al., 2008; Simpson et al., 2013; Beraldi-Campesi and Retallack, 2015). The Dayulin examples (Chu et al., 2015; this study) indicate that MISS-related microbial mats proliferated in the aftermath of the PTB extinction.

The Dayulin MISSs are all preserved in sandstone, with grain sizes varying from fine to very coarse. They are widely distributed in three facies associations: lake delta, riverbed/point bar setting, and flood plain. Although no major differences were observed in MISSs from these three facies associations, microbial record seems to be relatively fewer in lake delta settings probably because the widespread fine sediments (i.e. mudstone) prohibited the growth of MISS-related microbial mats. Besides, marine MISS-related microbial mats inhabit relatively calm conditions (Noffke, 2010). In contrast, the Dayulin MISS-related microbial mats colonize the riverbed sediments, which were deposited in a relatively high energy condition with upper flow regime. Paleosols in the sequence are clayey and have large drab-haloed root traces as evidence for woody vegetation that would have disrupted microbial mats in the likely Permian-Triassic boundary interval of the upper Sunjiagou Formation and in the clayey Heshanggou Formation.

6.3. Implications for post-extinction microbial proliferation in terrestrial ecosystems

Both modern MISS-related microbial mats and deep time examples have been interpreted to be created by the interaction of physical agents such as wind, wave and current with microbial organics (Noffke and Paterson, 2008; Noffke, 2010). Similar MISSs have also been widely reported from the marine Lower Triassic successions of western US and north Italy, and have been interpreted as indication of environmental stresses following the end-Permian great dying (Pruss et al., 2004, 2006; Mata and Bottjer, 2009a). Similarly, the Dayulin MISSs may indicate a devastated terrestrial ecosystem and environmental deterioration following the PTB biocrisis, but it is equally plausible that they reflect climatic change to semi-arid conditions.

More recently, Chu et al. (2015) proposed that microbial mats were oases for surviving aquatic animals, because the top layer of microbial mats generates oxygen, as revealed by analogy with modern microbial mats (Gingras et al., 2011; Tarhan et al., 2013). This scenario, however, is weakened by the failure to find any ostracods or other animal fossils directly from the wrinkled beds in the studied sections. This is also true for our field observations that all MISS-bearing horizons lack any animal body and trace fossils in Dayulin. Accordingly, the new observation and materials from Dayulin do not support Chu et al.'s (2015) oasis scenario for animal's survival in terrestrial ecosystems after the PTB mass extinction.

In contrast, the late Changhsingian part of the Sunjiagou Formation and Olenekian Heshanggou Formation are highly bioturbated and yield abundant burrows, but lack MISSs. Thus, it seems that the MISS-bearing habitats were not conducive for animals to inhabit. Whereas MISSs were very rare when animal activities were frequent. The proliferation of MISS-related microbial mats may indicate the degradation of terrestrial ecosystems or arid climate immediately after the severe Permian–Triassic mass extinction. The known materials indicate that terrestrial MISSs seem to be limited in Induan and disappeared in Olenekian. This phenomenon is also reinforced by our observations of three other sections in Henan Province. If so, the terrestrial ecosystems were likely devastated in Induan, but much improved in Olenekian. In contrast, marine MISSs occurred through the entire Early Triassic (Pruss et al., 2004, 2006; Mata and Bottjer, 2009a), indicating that recurrent devastation of marine ecosystems may have extended to the end of the Early Triassic, as supported by independent evidence from geochemical and geobiologic studies (Ezaki et al., 2012; Saito et al., 2014, 2015). However, these inferred differences between Early Triassic MISS in terrestrial and marine settings may be biased by the small number of studied sites and preservational states, and needs to be tested by additional studies on the Early Triassic terrestrial MISSs.

7. Conclusions

The present study on the Lower Triassic MISS from terrestrial ecosystems in North China clarified the following new observations of MISS relevant to their morphology, biogenicity, and implications on post-extinction environmental stresses:

(1) A total of six types of well-preserved MISSs are described from the Induan terrestrial successions exposed in the Dayulin section of Yiyang area, North China, including polygonal sand cracks, worm-like structures, wrinkle structures, sponge pore fabrics, gas domes and leveled ripple marks. They represent the first record of diverse MISSs in lacustrine and fluvial settings in Early Triassic, broadening microbial distribution to terrestrial settings in the geological past.
(2) Thin clayey laminae and filamentous mica grains arranged parallel to bedding plane as well as oriented sand quartz floating in lamina are the main features visible under the microscope, further supported by EDS-equipped SEM. Several lines of evidence indicate the Dayulin MISSs are created with the involvement of ancient microbes.
(3) Proliferation of MISS-related microbial mats, and rarity of metazoan animal fossils and burrows, may indicate environmental devastation and arid climate in the aftermath of Permian–Triassic biocrisis.

Acknowledgments

We thank B. Hu for his introduction of local geology in Yiyang area. We are also grateful to Brian Jones, Santanu Banerjee, and an anonymous reviewer for their critical comments and constructive suggestions that have greatly improved the quality of this paper. This study was supported by the 111 Program of China (B08030), Ministry of Education of China, a NSFC research grant (41272023), two research grants from the State Key Laboratory of Biogeology and Environmental Geology (GBL11206) and the State Key Laboratory of Geological Processes and Mineral Resources(GPMR201302), China University of Geosciences, and a research grant from Chengdu Center, China Geological Survey (12120113049100-1). It is a contribution to IGCP 630.

References

Allen, J.R.L., 1982. Sedimentary structures, their character and physical basis. Part II. Developments in Sedimentology Series. Elsevier, Amsterdam, pp. 1–676.
Banerjee, S., 2012. Discoidal microbial colonies. International Journal of Earth Sciences 101, 1343.
Banerjee, S., Jeevankumar, S., 2005. Microbially originated wrinkle structures on sandstone and their stratigraphic context: palaeoproterozoic Koldaha Shale, central India. Sedimentary Geology 176, 211–224.
Banerjee, S., Sarkar, S., Eriksson, P.G., Samanta, P., 2010. Microbially related structures in siliciclastic sediment resembling Ediacaran fossils: examples from India, ancient and modern. In: Seckbach, J., Oren, A. (Eds.), Microbial Mats: Modern and Ancient Microorganisms in Stratified Systems. Springer-Verlag, Berlin, pp. 111–129.
Banerjee, S., Sarkar, S., Eriksson, P.G., 2014. Palaeoenvironmental and biostratigraphic implications of microbial mat-related structures: examples from modern Gulf of Cambay and Precambrian Vindhyan basin. Journal of Palaeogeography 3, 127–144.
Baud, A., Richoz, S., Pruss, S., 2007. The Lower Triassic anachronistic carbonate facies in space and time. Global and Planetary Change 55, 81–89.
Benton, M.J., Tverdokhlebov, V.P., Surkov, M.V., 2004. Ecosystem remodelling among vertebrates at the Permian–Triassic boundary in Russia. Nature 432, 97–100.
Beraldi-Campesi, H., Retallack, G.J., 2015. In: Weber, B., Belnap, J., Büdel, B. (Eds.), Biocrusts Past and Present Precambrian terrestrial ecosystems. Springer, Berlin (in press).
Bose, S., Chafetz, H.S., 2009. Topographic control on distribution of modern microbially induced sedimentary structures (MISS): a case study from Texas coast. Sedimentary Geology 213, 136–149.
Bottjer, D., Hagadorn, J.W., 2007. Mat growth features. In: Schieber, J., Bose, P.K., Eriksson, P.G., Banerjee, S., Sarkar, S., Altermann, W., Catuneau, O. (Eds.), Atlas of Microbial Mat Features Preserved Within the Siliciclastic Rock Record, Atlases in Geosciences. Elsevier, Amsterdam, pp. 53–71.
Bouougri, E., Porada, H., 2002. Mat-related sedimentary structures in Neoproterozoic peritidal passive margin deposits of the West African Craton (Anti-Atlas, Morocco). Sedimentary Geology 153, 85–106.
Calner, M., 2005. A Late Silurian extinction event and anachronistic period. Geology 33, 305–308.
Chen, Z.Q., Benton, M.J., 2012. The timing and pattern of biotic recovery following the end-Permian mass extinction. Nature Geoscience 5, 375–383.
Chen, Z.Q., Wang, Y.B., Kershaw, S., Luo, M., Yang, H., Zhao, L.S., Fang, Y.H., Chen, J.B., Yang, L., Zhang, L., 2014. Early Triassic stromatolites in a siliciclastic nearshore setting in northern Perth Basin, Western Australia: geobiologic features and implications for post-extinction microbial proliferation. Global and Planetary Change 121, 89–100.
Cheng, Z.W., Qu, L.F., Hou, J.P., Li, P.X., 1983. The stratigraphic question of *Eumorphotis*-bearing 'Shiqianfeng' Formation in Qishan, Shaanxi Province. Journal of Stratigraphy 7, 161–168 (in Chinese).
Chu, D.L., Tong, J.N., Song, H.J., Benton, M.J., Bottjer, D.J., Song, H.Y., Tian, L., 2015. Early Triassic wrinkle structures on land: stressed environments and oases for life. Scientific Reports 5. http://dx.doi.org/10.1038/srep10109.
Davies, G.H. (Ed.), 1984. Structural Geology of Rocks and Regions. John Wiley and Sons, New York (491 pp.).
Eriksson, P.G., Porada, H., Banerjee, S., Bouougri, E., Sarkar, S., Bumby, A.J., 2007. Mat-destruction features. In: Schieber, J., Bose, P.K., Eriksson, P.G., Banerjee, S., Sarkar, S., Altermann, W., Catuneau, O. (Eds.), Atlas of Microbial Mat Features Preserved Within the Siliciclastic Rock Record, Atlases in Geosciences. Elsevier, Amsterdam, pp. 76–105.
Eriksson, P.G., Sarkar, S., Banerjee, S., Porada, H., Catuneanu, O., Samanta, P., 2010. Paleoenvironmental context of microbial mat-related structures in siliciclastic rocks: examples from the Proterozoic of India and South Africa. In: Seckbach, J., Oren, A. (Eds.), Microbial Mats: Modern and Ancient Microorganisms in Stratified Systems. Springer-Verlag, Berlin, pp. 73–108.
Erwin, D.H., 2006. Extinction: How Life on Earth Nearly Ended 250 Million Years Ago. Princeton University Press, Princeton, p. 296.
Ezaki, Y., Liu, J., Adachi, N., 2012. Lower Triassic stromatolites in Luodian County, Guizhou Province, South China: evidence for the protracted devastation of the marine environments. Geobiology 10, 48–59.
Frey, S.E., Gingras, M.K., Dashtgard, S.E., 2009. Experimental studies of gas-escape and water-escape structures: mechanisms and morphologies. Journal of Sedimentary Research 79, 808–816.
Garlick, W.G., 1988. Algal mats, load structures, and synsedimentary sulfides in Revett Quartzites of Montana and Idaho. Economic Geology 83, 1259–1278.
Gingras, M., Hagadorn, J.W., Seilacher, A., Lalonde, S.V., Pecoits, E., Petrash, D., Konhauser, K.O., 2011. Possible evolution of mobile animals in association with microbial mats. Nature Geoscience 4, 372–375.
Hagadorn, J.W., Bottjer, D.J., 1997. Wrinkle structures: microbially mediated sedimentary structures in siliciclastic settings at the Proterozoic–Phanerozoic transition. Geology 25, 1047–1050.

Hu, B., Yang, W.T., Song, H.B., Wang, M., Zhong, M.Y., 2009. Trace fossils and ichnofabrics in the Heshanggou Formation of lacustrine deposits, Jiyuan Area, Henan Province. Acta Sedimentologica Sinica 27, 573–582 (in Chinese).
Kalkowsky, E., 1908. Oolith und Stromatolith im norddeutschen Buntsandstein. Zeitschrift der Deutschen Geologischen Gesellschaft 60, 68–125.
Kershaw, S., Crasquin, S., Li, Y., Collin, P.Y., Forel, M.B., Mu, X., Baud, A., Wang, Y., Xie, S., Maurer, F., Guo, L., 2012. Microbialites and global environmental change across the Permian–Triassic boundary: a synthesis. Geobiology 10, 25–47.
Kirkland, B.L., Lynch, F.L., Rahnis, M.A., Folk, R.L., Molineux, I.J., McLean, R.J.C., 1999. Alternative origins for nanobacteria-like objects in calcite. Geology 27, 347–350.
Lan, Z.W., Chen, Z.Q., 2012. Exceptionally preserved microbially induced sedimentary structures from the Ediacaran post-glacial successions in the Kimberley region, northwestern Australia. Precambrian Research 200–203, 1–25.
Lan, Z.W., Chen, Z.Q., 2013. Proliferation of MISS-forming microbial mats after the late Neoproterozoic glaciations: evidence from the Kimberley region, NW Australia. Precambrian Research 224, 529–550.
Lan, Z.W., Chen, Z.Q., Li, X.H., Kaiho, K., 2013. Microbially induced sedimentary structures from the Mesoproterozoic Huangqikou Formation, Helan Mountain region, northern China. Precambrian Research 233, 73–92.
Li, Q.P., Wang, S.J., Wang, J.G., Yang, E.X., Zhang, C.C., Zhu, J.T., Xu, H., 2003. Discovery and age assignment of sporopollen in the Shiqianfeng Group in the Zhangqiu area, Shandong. Geological Bulletin of China 22, 346–350 (in Chinese).
Lin, L.Q., Fu, A.M., 1992. Preliminary research on strata from carboniferous to Jurassic of Shanxi Province. Journal of Central China Normal University (Natural Sciences) 26, 244–251 (in Chinese).
Liu, S.W., He, Z.J., 2000. Marine conchostracans from the 'Sunjiagou Formation' of Qishan, Shaanxi. Acta Palaeontologica Sinica 39, 230–236 (in Chinese with English abstract).
Liu, H.Y., Liu, X.T., 1984. Continental Triassic lithostratigraphic units in Shanxi Province–Shiqianfeng Group and Ermaying Group. Bulletin of the Chinese Academy of Geological Science 9, 137–156 (in Chinese).
Liu, C., Sun, B.L., Zeng, F.G., 2014. Constraints on U–Pb dating of detrital zircon of the maximum depositional age for Upper Permian to Lower Triassic strata in Xishan, Taiyuan. Acta Geologica Sinica 88, 1579–1587 (in Chinese with English abstract).
Lowe, D.R., 1975. Water escape structures in coarse-grained sediments. Sedimentology 22, 157–204.
Luo, M., Chen, Z.Q., Hu, S.X., Zhang, Q.Y., Benton, M.J., Zhou, C.Y., Wen, W., Huang, J.Y., 2013. Carbonate reticulated ridge structures from the lower middle Triassic of the Luoping area, Yunnan, Southwestern China: geobiological features and implications for exceptional preservation of the Luoping Biota. Palaios 28, 541–551.
Luo, M., Chen, Z.Q., Zhao, L.S., Kershaw, S., Huang, J.Y., Wu, L.L., Yang, H., Fang, Y.H., Huang, Y.G., Zhang, Q.Y., Hu, S.X., Zhou, C.Y., Wen, W., Jia, Z.H., 2014. Early Middle Triassic stromatolites from the Luoping area, Yunnan Province, Southwest China: Geologic features and environmental implications. Palaeogeography, Palaeoclimatology, Palaeoecology 412, 124–140.
Mariotti, G., Pruss, P.B., Perron, J.T., Bosak, T., 2014. Microbial shaping of sedimentary wrinkle structures. Nature Geoscience 7, 736–740.
Mata, S.A., Bottjer, D.J., 2009a. Development of Lower Triassic wrinkle structures: implications for the search for life on other planets. Astrobiology 9, 895–906.
Mata, S.A., Bottjer, D.J., 2009b. The paleoenvironmental distribution of Phanerozoic wrinkle structures. Earth-Science Reviews 3, 181–195.
Mazzoli, S., Carnemolla, S., 1993. Effects of the superposition of compaction and tectonic strain during folding of a multilayer sequence-model and observations. Journal of Structural Geology 15, 277–291.
McFadden, L.D., Wells, S.G., Anderson, K., Quade, J., Forman, S.L., 1998. The vesicular layer and carbonate collars of desert soils and pavements: formation, age and relation to climate change. Geomorphology 24, 101–145.
Mossman, D.J., Minter, W.E.L., Dutkiewiczc, A., Hallbauer, D.K., George, S.C., Hennigh, Q., Reimer, T.O., Horscroft, F.D., 2008. The indigenous origin of Witwatersrand "carbon". Precambrian Research 164, 173–186.
Noffke, N., 2009. The criteria for the biogenicity of microbially induced sedimentary structures (MISS) in Archean and younger, sandy deposits. Earth-Science Reviews 96, 173–180.
Noffke, N., 2010. Geobiology: Microbial Mats in Sandy Deposits from the Archean Era to Today. Springer, Berlin/London, p. 194.
Noffke, N., Paterson, D., 2008. Microbial interactions with physical sediment dynamics, and their significance for the interpretation of Earth's biological history. Geobiology 6, 1–4.
Noffke, N., Gerdes, G., Klenke, T., Krumbein, W.E., 1997. A microscopic sedimentary succession of graded sand and microbial mats in modern siliciclastic tidal flats. Sedimentary Geology 110, 1–6.
Noffke, N., Gerdes, G., Klenke, T., Krumbein, W.E., 2001. Microbially induced sedimentary structures — a new category within the classification of primary sedimentary structures. Journal of Sedimentary Research 71, 649–656.
Noffke, N., Knoll, A.H., Grotzinger, J.P., 2002. Sedimentary controls on the formation and preservation of microbial mats in siliciclastic deposits: a case study from the Upper Neoproterozoic Nama Group, Namibia. Palaios 17, 533–544.
Noffke, N., Hazen, R., Nhleko, N., 2003a. Earth's earliest microbial mats in a siliciclastic marine environment (2.9 Ga Mozaan Group, South Africa). Geology 31, 673–676.
Noffke, N., Gerdes, G., Klenke, T., 2003b. Benthic cyanobacteria and their influence on the sedimentary dynamics of peritidal depositional systems (siliciclastic, evaporitic salty and evaporitic carbonatic). Earth-Science Reviews 12, 1–14.
Noffke, N., Beukes, N., Bower, D., Hazen, R.M., Swift, D.J.P., 2008. An actualistic perspective into Archean worlds: (cyano-)bacterially induced sedimentary structures in the siliciclastic Nhlazatse Section, 2.9 Ga Pongola Supergroup, South Africa. Geobiology 6, 5–20.
Ouyang, S., Zhang, Z., 1982. Early Triassic palynological assemblage in Dengfeng, northwestern Henan. Acta Palaeontologica Sinica 21, 685–696 (in Chinese with English abstract).
Owen, G., 1996. Anatomy of a water-escape cusp in Upper Proterozoic Torridon Group sandstones, Scotland. Sedimentary Geology 103, 117–128.
Parizot, M., Eriksson, P.G., Aifa, T., Sarkar, S., Banerjee, S., Catuneanu, O., Altermann, W., Bumby, A.J., Bordy, E.M., Rooy, J.L.V., Boshoff, A.J., 2005. Suspected microbial mat-related crack-like sedimentary structures in the Palaeoproterozoic Magaliesberg Formation sandstones, South Africa. Precambrian Research 138, 274–296.
Peng, Z.M., Wu, Z.P., 2006. Development features of Triassic strata and analysis of original sedimentary pattern in North China. Geological Journal of China Universities 12, 343–352 (in Chinese with English abstract).
Porada, H., Bouougri, E.H., 2007. Wrinkle structures—a critical review. Earth-Science Reviews 81, 199–215.
Porada, H., Bouougri, E.H., 2008. Neoproterozoic trace fossils vs. microbial mat structures: examples from the Tandilia Belt of Argentina. Gondwana Research 13, 480–487.
Pruss, S.B., Fraiser, M., Bottjer, D.J., 2004. Proliferation of Early Triassic wrinkle structures: implications for environmental stress following the end-Permian mass extinction. Geology 32, 461–464.
Pruss, S.B., Corsetti, F.A., Bottjer, D.J., 2005. The unusual sedimentary rock record of the Early Triassic: a case study from the southwestern United States. Palaeogeography, Palaeoclimatology, Palaeoecology 222, 33–52.
Pruss, S.B., Bottjer, D.J., Corsetti, F.A., Baud, A., 2006. A global marine sedimentary response to the end-Permian mass extinction: examples from southern Turkey and the western United States. Earth-Science Reviews 78, 193–206.
Retallack, G.J., 2013. Permian and Triassic greenhouse crises. Gondwana Research 24, 90–103.
Riding, R., 1999. The term stromatolite: towards an essential definition. Lethaia 32, 321–330.
Saito, R., Oba, M., Kaiho, K., Schaeffer, P., Adam, P., Takahashi, S., Nara, F.W., Chen, Z.Q., Tong, J.N., Tsuchiya, N., 2014. Extreme euxinia just prior to the Middle Triassic biotic recovery from the latest Permian mass extinction. Organic Geochemistry 73, 113–122.
Saito, R., Kaiho, K., Oba, M., Fujibayashi, M., Tong, J.N., Tian, L., 2015. Predominance of Archaea-derived hydrocarbons in an Early Triassic microbialite. Organic Geochemistry 85, 66–75.
Sakar, S., Banerjee, S., Samanta, P., Chakraborty, P.P., Mukhopadhyay, S., Singh, A.K., 2014. Spectral variation of microbial mat records in siliciclastic rocks: examples from four Indian Proterozoic basins and their modern equivalents in Gulf of Cambay. Journal of Asian Earth Sciences 91, 362–377.
Samanta, P., Mukhopadhyay, S., Mondal, A., Sarkar, S., 2011. Microbial mat structures in profile: the Neoproterozoic Sonia Sandstone, Rajasthan, India. Journal of Asian Earth Sciences 40, 542–549.
Sarkar, S., Banerjee, S., Eriksson, P.G., 2004. Microbial mat features in sandstone illustrated. In: Eriksson, P.G., Altermann, W., Nelson, W., Mueller, D.R., Catuneanu, O. (Eds.), The Precambrian Earth: Tempos and Events. Elsevier, Amsterdam, pp. 673–675.
Sarkar, S., Banerjee, S., Samanta, P., Jeevankumar, S., 2006. Microbial mat-induced sedimentary structures and their implications: examples from Chorhat Sandstone, M.P., India. Journal of Earth Systems Science 115, 49–60.
Sarkar, S., Bose, P.K., Samanta, P., Sengupta, P., Eriksson, P.G., 2008. Microbial mat mediated structures in the Ediacaran Sonia Sandstone, Rajasthan, India, and their implications for Proterozoic sedimentation. Precambrian Research 162, 248–263.
Schieber, J., 1998. Possible indicators of microbial mat deposits in shales and sandstones: examples from the Mid-Proterozoic Belt Supergroup, Montana, U.S.A. Sedimentary Geology 120, 105–124.
Schieber, J., 1999. Microbial mats in terrigenous clastics: the challenge of identification in the rock record. Palaios 14, 3–12.
Schieber, J., 2004. Microbial mats in the siliciclastic rock record: a summary of diagnostic features. In: Eriksson, P.G., Altermann, D.R., Nelson, D.R., Mueller, W.E., Catuneanu, O. (Eds.), The Precambrian Earth: Tempos and Events. Elsevier, Amsterdam, pp. 663–673.
Schieber, J., Bose, P.K., Eriksson, P.G., Banerjee, S., Sarkar, S., Altermann, W., Catuneau, O., 2007. Atlas of Microbial Mat Features Preserved Within the Siliciclastic Rock Record, Atlases in Geosciences. Elsevier, Amsterdam (311 pp.).
Seilacher, A., 2007. Microbial mats on muddy substrates—examples of possible sedimentary features and underlying processes. In: Schieber, J., Bose, P.K., Eriksson, P.G., Banerjee, S., Sarkar, S., Altermann, W., Catuneau, O. (Eds.), Atlas of Microbial Mats Features Preserved within the Clastic Rock Record. Elsevier, Amsterdam, pp. 117–134.
Simpson, E.L., Heness, E., Bumby, A., Eriksson, P.G., Eriksson, K.A., Hilbert-Wolf, H.-L., Linnevelt, S., Malenda, H.F., Tshepiso Modungwa, T., Okaforba, O.J., 2013. Evidence for 2.0 Ga continental microbial mats in a paleodesert setting. Precambrian Research 237, 36–50.
Sur, S., Schieber, J., Banerjee, S., 2006. Petrographic observations suggestive of microbial mats from Rampur Shale and Bijaigarh Shale, Vindhyan Basin, India. Journal of Earth System Science 115, 61–66.
Tarhan, L.G., Planavsky, N.J., Laumer, C.E., Stolz, J.F., Reid, R.P., 2013. Microbial mat controls on infaunal abundance and diversity in modern marine microbialites. Geobiology 11, 485–497.
Tewari, R., Ram-Awatar, Pandita, S.K., McLoughlin, S., Agnihotri, D., Pillai, S.S.K., Singh, V., Kumar, K., Bhat, G.D., 2015. The Permian–Triassic palynological transition in the Guryul Ravine. Earth-Science Reviews 149, 49–62.
Walker, R.G., James, N.P. (Eds.), 1992. Facies Models: Response to Sea-Level Change. Geological Association of Canada, Ontario (409 pp.).
Wang, H.Z., 1985. Atlas of the Palaeogeography of China. SinoMaps Press, Beijing (283 pp (in Chinese)).
Wang, Z.Q., 1986. *Liulinia lacinulata*, a new male cone of cycads from latest Permian in Shanxi. Acta Palaeontologica Sinica 25, 610–616 (in Chinese with English abstract).
Wang, B., 1988. Division and correlation of upper Permian–lower Triassic in middle part of Henan and discussions of some geological topics. Petroleum Geology and Experiment 10, 142–158 (in Chinese).

Wang, R.N., 1997. New advance of the study of the Shiqianfeng Formation in western Henan. Geological Review 43, 200–209 (in Chinese).
Xu, H., Zhao, Z., Lu, F., Yang, Y., Tang, Z., Sun, G., Xu, Y., 2004. Tectonic evolution of the Nanhuabei area and analysis about its petroleum potential. Geotectonica et Metallogenia 28, 450–463 (in Chinese).
Xu, L., Zhang, C.J., Jia, S.H., Zhang, J.M., Lü, J.C., Pan, Z.C., Zhang, H.Q., Yan, G.S., 2015. Element Geochemistry and Palaeoenvironment of Permian–Triassic Stratum in the Huaigeda Hill of Dayu Town Jiyuan Basin, Henan Province. Acta Geologica Sinica 89, 137–148 (in Chinese with English abstract).
Yang, Z.Y., Yin, H.F., Lin, H.M., 1979. Marine Triassic faunas from Shihchienfeng Group in the northern Weihe River Basin, Shaanxi Province. Acta Palaeontologica Sinica 18, 465–474 (in Chinese with English abstract).
Yin, H.F., Lin, H.M., 1979. Marine Triassic faunas and the geologic time from Shihchienfeng Group in the northern Weihe River Basin. Journal of Stratigraphy 3, 233–241 (in Chinese).
Yu, H.Z., Lu, F.L., Guo, Q.X., Lu, W.Z., Wu, J.Y., Han, S.H., 2005. Proto sediment basin types and tectonic evolution in the southern edge of North China Plate. Petroleum Geology and Experiment 27, 111–117 (in Chinese).
Yu, J.X., Broutin, J., Chen, Z.Q., Shi, X., Li, H., Chu, D.L., Huang, Q.S., 2015. Vegetation changeover across the Permian–Triassic boundary in southwest China: extinction, survival, recovery and paleoclimate: a critical review. Earth-Science Reviews 149, 199–220.
Yuan, A.H., Zhu, Z.M., Lin, W.J., Liu, Y.Y., 2003. Susceptibility study on the boundary of terrestrial Permian–Triassic in Ningwu, Shanxi Province. Geological Science and Technology Information 22, 37–40 (in Chinese).
Zhang, K., 1991. Diachronism of the Sunjiagou Formation—a discussion. Regional Geology of China 3, 221–228 (in Chinese).
Zhang, S.F., Zhang, Z.Q., Song, Z.Y., Gao, M.X., 1994. Stratigraphic division and correlation of the Carboniferous, Permian and Triassic strata in Shandong Province. Shandong Geology 10, 46–52 (in Chinese).
Zhang, L., Yang, W., Niu, Y., 2014. Characteristic and geological significance of microbially induced sedimentary structures (MISS) in terrestrial P–Tr boundary in western Henan. Acta Geologica Sinica 60, 1051–1060 (in Chinese with English abstract).
Zhao, Z.Q., Shi, C.L., Zhao, J., Feng, Y.Q., 1980. Triassic *Charophytes* from Liaocheng of Shandong and Linxi of Hebei. Acta Palaeontologica Sinica 19, 412–414 (in Chinese with English abstract).
Zhu, R., Xu, H., Deng, S., Guo, H., 2007. Lithofacies palaeogeography of the Permian in northern China. Journal of Palaeogeography 9, 133–142 (in Chinese with English abstract).